Climate Resilience and Sustainability
Open Access
Interdisciplinary Approaches Towards Solutions for Climate Change
RMetS
Royal Meteorological Society

ORIGINAL ARTICLE

Assessing the representation of South American monsoon features in Brazil and U.K. climate model simulations

Caio A. S. Coelho[1] (ORCID) | **Dayana C. de Souza[1]** | **Paulo Y. Kubota[1]** |
Iracema F. A. Cavalcanti[1] | **Jessica C. A. Baker[2]** | **Silvio N. Figueroa[1]** |
Mári A. F. Firpo[1] | **Bruno S. Guimarães[1]** | **Simone M. S. Costa[1]** |
Layrson J. M. Gonçalves[1] | **José P. Bonatti[1]** | **Gilvan Sampaio[1]** |
Nicholas P. Klingaman[3,4] | **Amulya Chevuturi[3,4,5]** (ORCID) | **Martin B. Andrews[6]**

[1] Centro de Previsão de Tempo e Estudos Climáticos (CPTEC), Instituto Nacional de Pesquisas Espaciais (INPE), Cachoeira Paulista, Brazil

[2] Institute for Climate and Atmospheric Science, School of Earth and Environment, University of Leeds, Leeds, UK

[3] National Centre for Atmospheric Science, University of Reading, Reading, UK

[4] Department of Meteorology, University of Reading, Reading, UK

[5] UK Centre for Ecology and Hydrology, Wallingford, UK

[6] UK Met Office, Exeter, UK

Correspondence
Caio A. S. Coelho, Centro de Previsão de Tempo e Estudos Climáticos (CPTEC), Instituto Nacional de Pesquisas Espaciais (INPE), Rodovia Presidente Dutra, Km 40, SP-RJ, Cachoeira Paulista, SP 12630-000, Brazil.
Email: caio.coelho@inpe.br

Abstract

This paper assesses how well the CPTEC/INPE Brazilian Global Atmospheric Model (BAM-1.2) and the atmospheric component of the UK Met Office Hadley Centre Global Environment Model (HadGEM3-GC3.1) represent the main South American monsoon features. Climatological (1981–2010) ensemble means of Atmospheric Model Intercomparison Project (AMIP)-type climate simulations are evaluated. The assessment evaluated the models' ability to represent the South America austral summer and winter precipitation contrast and associated circulation, key South American monsoon system elements, the association between south-east Brazil and South America precipitation, and climatological (1997/1998 to 2013/2014) distributions of rainy season onset and demise dates over south-east Brazil (15°S–25°S, 40°W–50°W) and the core monsoon region (10°S–20°S, 45°W–55°W). Despite some identified deficiencies, both models depict the monsoon region and represent the main features, including (1) the north-west–south-east precipitation band and associated ascending motion over central South America; (2) the upper-level Bolivian High and the north-east South America trough during the summer; (3) the lower-level South Atlantic and Pacific subtropical anti-cyclones and (4) the low-level jet east of the Andes. Both models represent upper-level divergence and lower-level convergence over the

2 | **Climate Resilience and Sustainability**
Interdisciplinary Approaches Towards Solutions for Climate Change
Open Access
RMetS

COELHO ET AL.

core monsoon region, and upper-level convergence and lower-level divergence over the Pacific and Atlantic anti-cyclones associated with the regional Walker circulation during the pre-monsoon (spring) and peak monsoon (summer) seasons. Convection over South America is weaker in BAM-1.2 than observed, consistent with continental precipitation deficit. The models reproduce the dipole-like precipitation pattern between south-east Brazil and south-eastern South America during the austral summer but overestimate these patterns spatial extent over the South Atlantic. Both models simulate the main observed climatological features of rainy season onset and demise dates for the two above defined investigated regions. HadGEM3 overestimates onset dates interannual variability. These results can contribute towards understanding climate and land-use change implications for environmental sustainability and for recommending climate adaptation strategies.

KEYWORDS
climate model evaluation, rainy season onset and demise, South America monsoon

1 | INTRODUCTION

A large proportion of the South American continent has a monsoon-like precipitation regime with a wet season during the austral summer months (December, January and February, DJF) and a dry season during the austral winter months (June, July and August, JJA) (Jones and Carvalho, 2002). The monsoon is one of the most important climate phenomena for the region in terms of both scientific and societal interests. The great majority of the South American population lives in regions directly affected by its monsoon climate features. Several activities can be affected by negative precipitation anomalies occurring during the wet season. For example, agricultural production can be reduced, navigation in rivers can be halted, hydropower generation can be compromised and bush fires can spread and affect biodiversity in addition to air transport and public health (Marengo et al., 2008; Zeng et al., 2008; Marengo et al., 2011; Espinoza et al., 2011). Similarly, positive precipitation anomalies may lead to severe flood events (Marengo and Espinoza, 2016; Barichivich et al., 2018). Hence, monsoon climate variability directly impacts the livelihood of the South American population. It is therefore fundamental to have a solid understanding of the climate features of the South American monsoon, including aspects of the atmospheric circulation, and how they are represented in climate models, with the latter used to both simulate past climate conditions and predict future conditions. This knowledge is important for offering society credible information to help build resilience and a sustainable future.

Several studies have documented various aspects of the South American monsoon system (SAMS; Vera et al., 2006; Marengo et al., 2012; Silva and Kousky, 2012). The monsoon system is characterized by changes in atmospheric circulation and precipitation from winter to summer, resulting in the establishment of the South Atlantic Convergence Zone (SACZ; Kodama, 1992; 1993), the Bolivian High and the upper-level trough over north-east South America (sometimes referred to as the north-east Brazil trough) during the mature phase. At lower levels, the moisture flux from the Atlantic and the Amazon region contributes to enhancing convective activity and precipitation over central and south-east Brazil. Raia and Cavalcanti (2008) discussed atmospheric circulation features associated with the SAMS initiation and end. During the initiation stage, atmospheric pressure decreases over the continent as the subtropical South Atlantic high-pressure system displaces eastward, moving away from the continent, and a strong north-westerly moisture flux develops to the east of the tropical Andes towards south-east Brazil. During the end stage, the subtropical South Atlantic high-pressure system displaces westward, moving towards South America and leading to increased atmospheric pressure over the continent and the cessation of the moisture flux towards south-east Brazil. The SAMS onset and demise dates are features of particular interest to several authors. These features have been identified using different methods and variables, such as outgoing longwave radiation (Kousky, 1988), precipitation (Liebmann and Marengo, 2001), precipitation and zonal wind (Gan et al., 2004), a combination of precipitation, specific humidity, air temperature and zonal and

meridional winds (Silva and Carvalho, 2007) and humidity flux (Raia and Cavalcanti, 2008). A compilation and description of all these methods is provided in Carvalho and Cavalcanti (2016).

Atmospheric and coupled ocean-atmosphere climate models have been analysed to investigate their capabilities in representing the main SAMS features. Cavalcanti and Raia (2017) reported that climate simulations produced with the Center for Weather Forecast and Climate Studies (CPTEC/INPE) Atmospheric Global Circulation Model (AGCM) were able to represent the atmospheric patterns associated with SAMS initiation and end phases, although with different intensities with respect to the observations. Cavalcanti et al. (2020) showed that the Brazilian Atmosphere Global Model (BAM-v0) depicted the SAMS domain with climate simulations reproducing a similar spatial extent as identified in observations, and adequately represented precipitation and humidity flux differences between summer and winter. Although the spatial patterns simulated by the model were similar to the observed patterns, precipitation and moisture convergence were underestimated when compared to the observations, particularly over the Amazon region. Díaz et al. (2020) reported that only a few models of the Coupled Model Intercomparison Project Phase 6 (CMIP6) were able to represent the observed climatological precipitation pattern during the SAMS mature phase in austral summer. This deficiency had previously been noticed in CMIP5 models (Jones and Carvalho, 2013). Most CMIP5 and CMIP6 models misplaced the location of the maximum climatological precipitation over South America during the summer. However, Carvalho and Cavalcanti (2016) reported that a selection of five CMIP5 models presented a plausible representation of the summer and winter precipitation climatological patterns over South America. The precipitation annual cycle over the core South American monsoon region was well represented by these five models, although biases were identified. García-Franco et al. (2020) reported that two CMIP6 models (HadGEM3-GC3 and UKESM1) simulated the main summer monsoon precipitation and lower-level wind features; however, precipitation was underestimated over north-west South America and overestimated over other SAMS regions. With respect to the SAMS lifecycle, Kitoh et al. (2013) reported that CMIP5 models presented longer than observed duration, due to simulations indicating earlier than observed onsets and later than observed demises.

This study aims to assess how well the CPTEC/INPE Brazilian Global Atmospheric Model version 1.2 (BAM-1.2; Coelho et al., 2021) and the atmospheric component of the UK Met Office Hadley Centre Global Environment Model version 3 (HadGEM3-GC3.1; Ridley et al., 2018; Williams et al., 2018) represent the main features of the South American Monsoon system in Atmospheric Model Intercomparison Project (AMIP)-type climate simulations. The UK Met Office model simulations will hereafter be referred to as HadGEM3 for brevity. In order to achieve this aim, for most of the analysis performed in this study, we compare observed and model-simulated climatological ensemble means of four BAM-1.2 ensemble members and five HadGEM3 ensemble members for selected variables over the 1981–2010 period (see Section 2 for additional information on the methodology used in the performed evaluation). More specifically, in this study we investigate and document how well the two models represent the following features:

- South America monsoon precipitation contrast between summer and winter and associated circulation features (Section 3);
- Key elements of the South American monsoon system (Section 4);
- Associations between precipitation in south-east Brazil and elsewhere in South America (Section 5) and
- Climatological distributions of rainy season onset and demise dates over south-east Brazil and the core South America monsoon region (Section 6).

Assessment studies as performed here provide confidence for the use of climate models in future research to help society deal with climate variability and its associated impacts, including supporting the definition of recommendations and policies for climate adaptation to improve societal resilience to climate change. Besides, identified model deficiencies can be used to drive model developments and further improve predictive capabilities.

2 | DATA AND METHODS

2.1 | Observational data sets

Precipitation data from the Global Precipitation Climatology Project (GPCP) v2.3 (Adler et al., 2003) available at monthly time resolution for the 1981–2010 period, and from GPCP version v1.3 (Huffman et al., 2001) at daily time resolution, which is available for 1997 onwards, were used in the evaluation of precipitation features associated with the South American monsoon system, including the estimation of rainy season onset and demise dates using daily precipitation. The fifth generation of the European Centre for Medium-range Weather Forecasts (ECMWF) atmospheric reanalysis of the global climate (ERA5; Hersbach et al., 2020) data set available at monthly time resolution for the 1981–2010 period was used for evaluating circulation, humidity and top of the atmosphere outgoing

4 | **Climate Resilience and Sustainability**
Interdisciplinary Approaches Towards Solutions for Climate Change | Open Access | RMetS

COELHO ET AL.

longwave radiation features associated with the South American monsoon system.

2.2 | Climate model simulations

AMIP-type climate simulations produced with BAM-1.2 (Coelho et al., 2021) and HadGEM3 (Ridley et al., 2018; Williams et al., 2018) were used in this study. The readers can find detailed descriptions about these two models, including information about the atmospheric initial conditions and configurations in terms of parameterizations used for producing the climate simulations evaluated in this study in Coelho et al. (2021), Ridley et al. (2018) and Williams et al. (2018). These simulations are produced using observed sea surface temperature and sea ice prescribed as boundary conditions for the global atmospheric models during the entire climate simulation period. A total of four ensemble members for BAM-1.2 and five ensemble members for HadGEM3 were used in the performed assessment. The horizontal spatial resolution in degrees of latitude and longitude is $1° \times 1°$ and ~$0.6° \times 0.6°$ for BAM-1.2 and HadGEM3, respectively. The performance of these two models in representing land–atmosphere interactions over South America has recently been documented in Baker et al. (2021).

2.3 | Monsoon precipitation intensity index

The monsoon precipitation intensity (MPI; Wang et al., 2011) index defined as the ratio between the annual range [AR; computed here as the difference between austral summer (DJF) and austral winter (JJA) mean precipitation] and the annual mean (AM) precipitation was used for mapping the spatial extent of the South American monsoon system, where the DJF, JJA and annual mean values were computed over the 1981–2010 period.

2.4 | Climatological means, model biases and spatial pattern association

Climatological means of observed and ensemble mean model simulations for selected variables were computed over the 1981–2010 period for all investigated seasons. Biases in model simulations were estimated by computing the difference between the climatological means of model-simulated and observed variables [e.g., precipitation, zonal and meridional wind components, vertical velocity (omega), sea level pressure, specific humidity] computed over the 1981–2010 period. To assess the strength of lin-

ear spatial pattern association between the simulated and observed climatological mean patterns, the pattern correlation value was computed for a number of circulation, precipitation, humidity and top of the atmosphere outgoing longwave radiation fields and vertical cross-sections. For atmospheric variables involving meridional and zonal wind components, these two components were combined prior to the computation of the pattern correlation.

2.5 | Non-rotational or divergent wind component

Using Helmholtz theorem, any wind vector $\vec{V} = u\vec{i} + v\vec{j}$ can be expressed as $\vec{V} = \vec{\nabla} \chi + \vec{k} \times \vec{\nabla}\psi$, where u and v are the zonal and meridional wind components, respectively. $\vec{V}_\chi = \vec{\nabla}\chi$ is the divergent (non-rotational) wind component, and χ is a variable defined as velocity potential. $\vec{V}_\psi = \vec{k} \times \vec{\nabla}\psi$ is the rotational wind component, and ψ is a variable defined as stream function. And $\vec{i}$, $\vec{j}$ and $\vec{k}$ are unit vectors in the east-west (x), north-south (y) and vertical (z) directions, respectively. In this study, to investigate the South American monsoon circulation features associated with divergence or convergence at 850 and 200 hPa, velocity potential χ and the divergent (non-rotational) wind component $\vec{V}_\chi$ were evaluated.

2.6 | Significance test for the difference in climatological mean values

For the investigation of whether the 1981–2010 climatological mean values of observed ($\bar{X}_o$) and ensemble mean model simulations ($\bar{X}_m$) were statistically significantly different from each other, the t-test was performed. This is a test for the null hypothesis of no difference between the two mean values against the alternative hypothesis of the existence of difference between the two mean values. The test was performed by computing the t statistic as follows:

$$t = \frac{\bar{X}_m - \bar{X}_o}{\sqrt{\frac{s_m^2}{n} + \frac{s_o^2}{n}}}, \quad (1)$$

where s_o and s_m are the observed and model simulations standard deviation values computed for $n = 30$ values in all analyses of this study. The associated degrees of freedom ν was estimated as follows:

$$\nu = \frac{\left(\frac{s_m^2}{n} + \frac{s_o^2}{n}\right)^2}{\frac{s_m^4}{n^2(n-1)} + \frac{s_o^4}{n^2(n-1)}}. \quad (2)$$
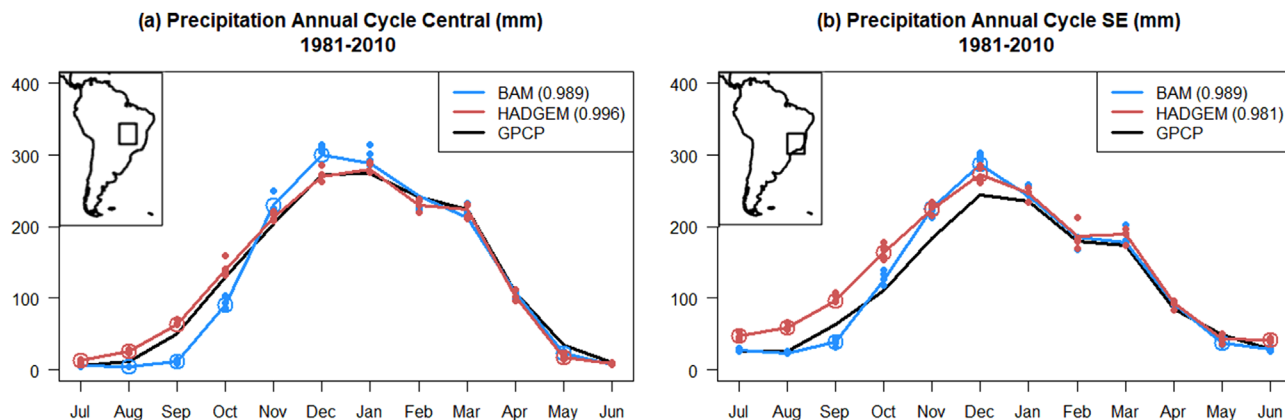
FIGURE 1 Climatological mean (1981–2010) monthly accumulated precipitation (mm) from July to June averaged over (a) the central South America region (10°S–20°S, 45°W–55°) and (b) part of south-east Brazil region (15°S–25°, 40°W–50°W). The regions over which precipitation was averaged are illustrated by the squares drawn on the South America maps shown on the top left corner of each figure panels. The lines describe the precipitation annual cycle derived from the observations (black line for GPCP v2.3) and from the ensemble means of the two climate models (blue line for BAM-1.2 and red line for HadGEM3). The blue and red dots represent the ensemble members for BAM-1.2 and HadGEM3, respectively. The open circles indicate the months for which the difference between the model ensemble mean and observed values was found to be statistically significant at the 5% level using the t-test for the null hypothesis of no difference between the climatological mean values (p-values < 0.05). The numbers in brackets displayed in the legends of both panels are the correlation values between the model ensemble mean (blue and red lines) and the observed (black line) annual cycles

The probability value (p-value) for the two-sided t-test was determined using the t-distribution with ν degrees of freedom by computing and summing the areas below the probability density function (PDF) curve of the t-distribution to the left of the value $-t$ and to the right of the value t. The test was performed by choosing the statistical significance level α equals to 5%. Therefore, when the p-values were found to be less than 5% the null hypothesis of no difference between the two mean values was rejected in favour of the alternative hypothesis, indicating that in such situations there was evidence for identifying differences in the investigated mean values.

3 | SOUTH AMERICA MONSOON PRECIPITATION CONTRAST AND ASSOCIATED CIRCULATION FEATURES

This section assesses how well the two investigated models (BAM-1.2 and HadGEM3) represent the monsoon precipitation contrast between summer and winter and the associated circulation features.

Figure 1 shows the climatological mean (1981–2010) precipitation annual cycle from July to June for the spatial average over two regions [10°S–20°S, 45°W–55°W in central South America and 15°S–25°S, 40°W–50°W over part of the south-east (SE) region in Brazil] as represented by the observations (black line for GPCP v2.3; Adler et al., 2003) and by the ensemble mean of the two investigated models (blue line for BAM-1.2 and red line for HadGEM3).

Both regions show a peak in precipitation during the austral summer (DJF) contrasting with much reduced precipitation during the austral winter (JJA). This contrast illustrates the monsoon-like precipitation feature of these regions in South America. The two models adequately represent the precipitation annual cycle with large correlation values (above 0.98) between the model ensemble mean (blue and red lines) and the observed (black line) annual cycles; however, deficiencies are also noticed. After performing a statistical significance t-test on the differences between the model ensemble mean and observed climatological mean values for each month for the null hypothesis of no difference at the 5% level, the following can be reported. BAM-1.2 underestimates precipitation in May and from August to October, and overestimates precipitation in November and December over the central South America region, whereas HadGEM3 underestimates precipitation in May and overestimates precipitation from July to September (Figure 1a). Over SE Brazil, HadGEM3 overestimates precipitation from June to December; BAM-1.2 underestimates precipitation in May and September and overestimates precipitation from October to December (Figure 1b). Figure 1a also shows that the spread of the ensemble members (blue and red dots) is larger from October to March for both models, consistent with the higher precipitation variability during austral summer when compared to winter (Table 1).

Table 1 shows climatological (1981–2010) mean precipitation values and MPI (Wang et al., 2011) index computed using observations (GPCP v2.3), BAM-1.2 and HadGEM3

6 | Climate Resilience and Sustainability
Interdisciplinary Approaches Towards Solutions for Climate Change · Open Access · RMetS Royal Meteorological Society

COELHO ET AL.

TABLE 1 Climatological (1981–2010) mean precipitation values and monsoon precipitation intensity (MPI) index computed using observations (second column, GPCP v2.3, Adler et al., 2003), BAM-1.2 (third column) and HadGEM3 (fourth column) averaged over the central South America region (10°S–20°S, 45°W–55°W)

	Observations (GPCP)	BAM-1.2	HadGEM3
DJF mean (mm)	262.8 (40.2)	277.0 (23.1)	260.1 (30.8)
JJA mean (mm)	9.5 (6.5)	**6.1** (2.4)	**16.1** (7.3)
Annual range (mm)	253.3 (41.1)	270.9 (23.6)	244.0 (32.3)
Annual mean (mm)	130.7 (13.3)	127.1 (8.3)	132.4 (12.1)
MPI	1.9 (0.2)	**2.1** (0.1)	1.8 (0.2)

Note: First two lines: Mean precipitation (mm) defined as the average value over the austral summer (DJF) and winter (JJA) months. Third line: Annual range (mm) defined as the difference between the austral summer (DJF) and winter (JJA) mean precipitation (i.e. the difference between the values of the first and second lines). Fourth line: Annual mean precipitation (mm) defined as the average of all 12 months of the year. Fifth line: MPI defined as the ratio between the annual range (third line) and the annual mean (fourth line). The values in brackets represent interannual variability estimates (i.e. standard deviations computed over the 1981–2010 period). The mean values highlighted in bold are statistically significant different at the 5% level from the mean observed values (first column) according to the *t*-test for the null hypothesis of no difference in the climatological mean values (*p*-values < 0.05).

averaged over the central South America region (10°S–20°S, 45°W–55°W). The mean precipitation values shown in the first two lines are defined as the average over the austral summer (DJF) and winter (JJA) months, respectively. The annual range shown in the third line is defined as the difference between the austral summer (DJF) and winter (JJA) mean precipitation. The annual mean precipitation shown in the fourth line is defined as the average of all 12 months of the year. As introduced in Section 2.3, following Wang et al. (2011), the MPI shown in the fifth line is defined as the ratio between the annual range (third line) and the annual mean (fourth line). The annual range provides a simple measure of monsoon strength, and the MPI is a complementary measure of monsoon strength relative to the annual mean precipitation. The observed annual range (253.3 mm) and annual mean (130.7 mm) lead to an MPI value of 1.9, indicating that the annual range is approximately double the annual mean value. The comparison of columns 2 and 3 in Table 1 reveals that BAM-1.2 overestimates the observed annual range and slightly underestimates the observed annual mean, leading to an overestimation of the MPI value (2.1). The comparison of columns 2 and 4 in Table 1 reveals that HadGEM3 underestimates the observed annual range value, and slightly overestimates the observed annual mean value, leading to a slight underestimation in the MPI value (1.8). The statistical significance assessment (using the *t*-test) on the difference of the climatological mean MPI values of the two investigated models with respect to the observed climatological mean MPI for the null hypothesis of no difference revealed that the difference was only statistically significant at the 5% level for BAM-1.2.

Figure 2 shows MPI maps computed over the climatological (1981–2010) period using observations (panel a, GPCP v2.3), and the ensemble means of the two investigated climate models [panel b (BAM-1.2) and panel c (HadGEM3)]. Both models depict the South American monsoon region through MPI values greater than or equal to 1.5 (i.e. the region where the annual range represents the annual mean value plus additional 50% of this annual mean value). The MPI pattern correlation computed between the models and observed (GPCP) MPI values over South America is above 0.89 for both models, highlighting the ability of the models to represent the spatial structure of monsoon precipitation. The box drawn over the central South America region (10°S–20°S, 45°W–55°W) illustrates the core monsoon region for which the climatological annual cycle is shown in Figure 1a and statistics are shown in Table 1.

Atmospheric circulation (winds) is another important component of monsoon systems. Figure 3 shows the climatological mean (1981–2010) seasonally accumulated precipitation and seasonal mean 850 hPa vector wind for austral summer (DJF, first row) and winter (JJA, second row) computed using observations (first column, GPCP v2.3 and ERA5 reanalysis; Hersbach et al., 2020) and the ensemble means of the two investigated climate models [second column (BAM-1.2) and third column (HadGEM3)]. Unlike in other monsoon regions (e.g. Asia), where a clear reversal of wind direction occurs between the ocean and the continent during the wet (summer, DJF) and dry (winter, JJA) seasons, the South American monsoon lacks this feature. During both seasons, winds blow from the Atlantic towards the continent following the prevailing anticyclonic circulation over the subtropical South Atlantic Ocean. During the summer, this anticyclonic circulation favours humidity transport from the ocean towards the continent, which is recycled over the Amazon forest region (Zemp et al., 2014) and diverted southwards establishing the low-level jet east of the Andes (Marengo et al., 2004). This circulation-driven humidity transport contributes to the establishment of the rainy season in central South America. During the winter, this humidity transport east of the Andes is predominantly meridional, reaching the south-east portion of
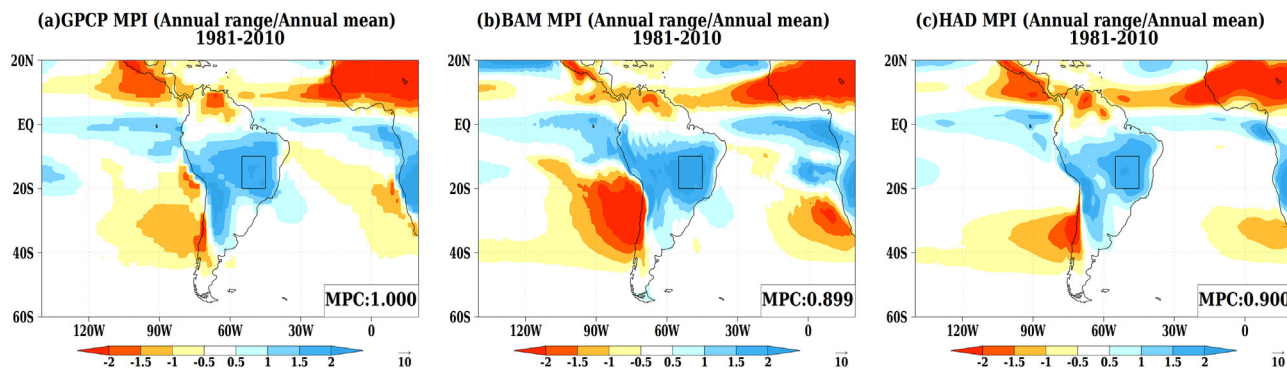
COELHO ET AL.

Climate Resilience and Sustainability
Interdisciplinary Approaches Towards Solutions for Climate Change   Open Access   RMetS   7

FIGURE 2   Monsoon precipitation intensity (MPI) index defined as the ratio between the climatological (1981–2010) mean annual range [summer (DJF) minus winter (JJA) mean precipitation] and the climatological (1981–2010) annual mean precipitation using observations (panel a, GPCP v2.3), and the ensemble means of the two investigated climate models [panel b (BAM-1.2) and panel c (HadGEM3)]. The box over central South America (10°S–20°S, 45°W–55°W) illustrates the core monsoon region. The numbers at the bottom right corners of each panel are the MPI pattern correlation (MPC) values computed between the models and observed (GPCP) MPI values over South America shown in these figure panels
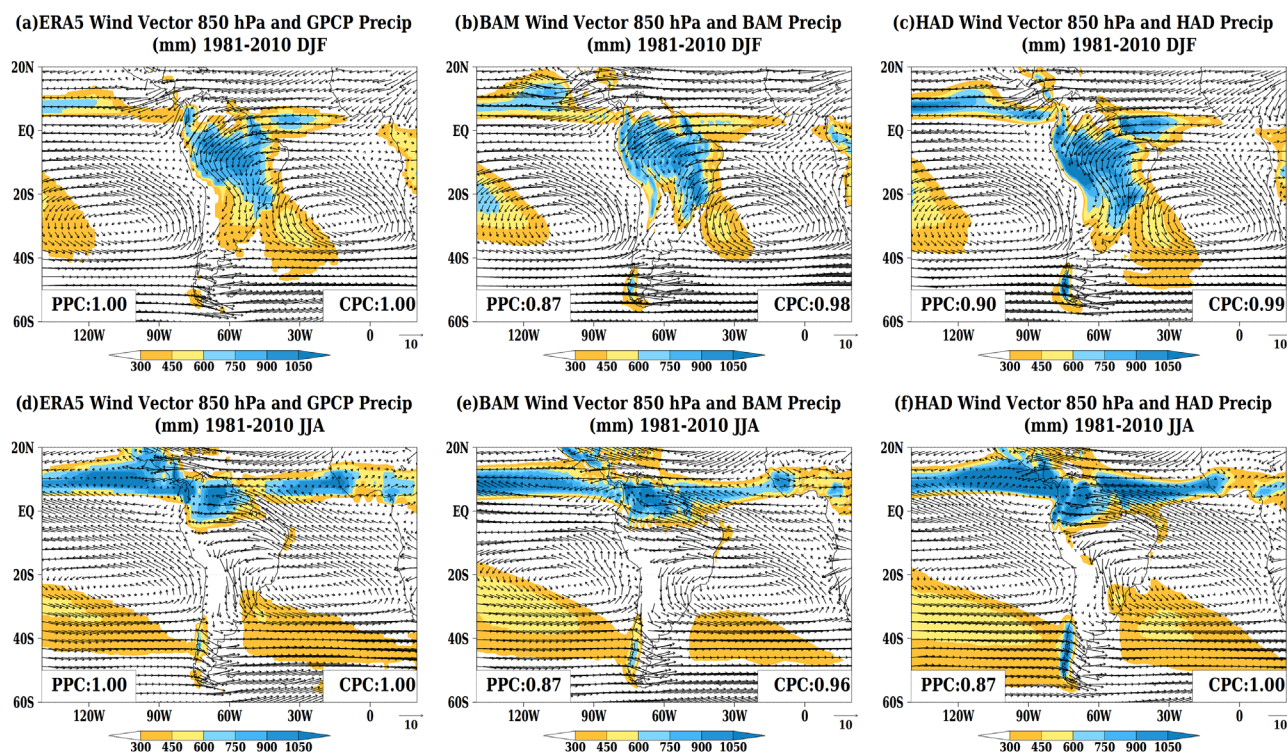

FIGURE 3   Climatological mean (1981–2010) seasonally accumulated precipitation (shaded, mm) and seasonal mean 850 hPa vector wind (arrows, m·s⁻¹) for austral summer (DJF, first row) and winter (JJA, second row) computed using observations (first column, GPCP v2.3 and ERA5) and the ensemble means of the two investigated climate models [second column (BAM-1.2) and third column (HadGEM3)]. The numbers at the bottom right corners of each panel are the circulation pattern correlation (CPC) values computed between the models and ERA5 zonal and meridional wind components values shown in these figure panels. The numbers at the bottom left corners of each panel are the precipitation pattern correlation (PPC) values computed between the models and observed (GPCP) values shown in these figure panels

South America where precipitation is favoured, whereas central South America experiences the dry season. Figure 3 shows that both models adequately represent the circulation and precipitation climatological features over South America described above during the wet (summer) and dry (winter) periods, with precipitation pattern correlation (PPC) values above 0.87 and circulation pattern correlation (CPC) values above 0.96 for both models. However, BAM-1.2 tends to underestimate precipitation over southeast South America and HadGEM3 tends to overestimate
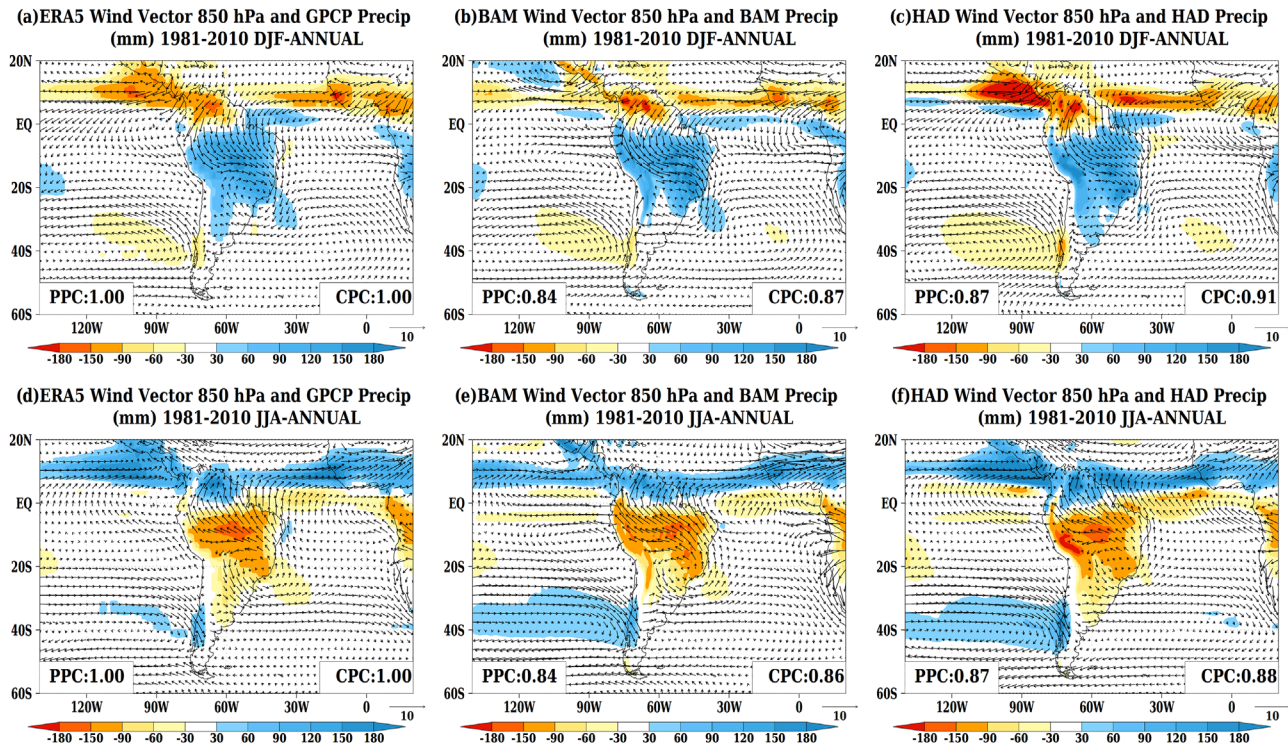
8 | Climate Resilience and Sustainability
Interdisciplinary Approaches Towards Solutions for Climate Change
Open Access
RMetS
Royal Meteorological Society
COELHO ET AL.

FIGURE 4 Climatological mean (1981–2010) difference between the mean precipitation over the austral summer (DJF, first row) and winter (JJA, second row) months and the annual mean precipitation (shaded, mm), and corresponding climatological mean differences between seasonal and annual mean 850 hPa vector wind (arrows, m·s^{-1}) computed using observations (first column, GPCP v2.3 and ERA5) and the ensemble means of the two investigated climate models [second column (BAM-1.2) and third column (HadGEM3)]. The numbers at the bottom right corners of each panel are the circulation pattern correlation (CPC) values computed between the models and ERA5 zonal and meridional wind components values shown in these figure panels. The numbers at the bottom left corners of each panel are the precipitation pattern correlation (PPC) values computed between the models and observed (GPCP) precipitation difference values shown in these figure panels

precipitation over this region, particularly during the summer. This model behaviour is associated with a slightly weaker than observed low-level jet east of the Andes in BAM-1.2 and a stronger than observed low-level jet in HadGEM3 (see Figure S1).

Figure 4 shows the climatological mean (1981–2010) difference between the mean precipitation over the austral summer (DJF, first row) and winter (JJA, second row) months and the annual mean precipitation, and the corresponding climatological mean differences between seasonal and annual mean 850 hPa vector wind (arrows) computed using observations (first column, GPCP v2.3 and ERA5) and the ensemble means of the two investigated climate models [second column (BAM-1.2) and third column (HadGEM3)]. Figure 4 shows that these differences with respect to the annual mean highlight circulation and precipitation contrasts between summer (DJF) and winter (JJA), including an apparent circulation reversal in the core monsoon region as previously reported in Zhou and Lau (1998), with a cyclonic feature during the summer (DJF) and an anti-cyclonic feature during the winter (JJA). All these features are appropriately repre-

sented by both models, with PPC values above 0.84 and CPC values above 0.86. Weak precipitation and circulation biases were identified over most of South America in both models (see Figure S2).

4 | KEY ELEMENTS OF THE SOUTH AMERICAN MONSOON SYSTEM

As identified in the previous section, precipitation over the core region of the South American monsoon (Figure 1a) peaks during the austral summer (DJF). It is noted, however, that precipitation starts to gradually increase from September. Therefore, it is important to characterize the atmospheric conditions during both the austral spring (the pre-monsoon season, September–October–November, SON) and the austral summer (the peak monsoon season, DJF) to better diagnose the elements contributing to the establishment of the peak monsoon precipitation over South America. This section identifies some of the key elements of the South American monsoon system during the pre-monsoon (SON) and peak monsoon (DJF) seasons and

assesses how well the two investigated models (BAM-1.2 and HadGEM3) represent these elements.

Figure 5a shows the climatological (1981–2010) seasonal mean upper level (200 hPa) circulation (streamlines) and accumulated seasonal precipitation (shaded) for the pre-monsoon season (SON) derived from ERA5 and GPCP v2.3. The upper-level Bolivian high circulation is noticed as an anticyclone located over South America, with an associated trough over the north-eastern part of South America. A north-west–south-east precipitation band is also identified over the South American continent. This band illustrates the signature of the South Atlantic convergence zone (Kodama, 1992, 1993), which is recognized as one of the main phenomena contributing to the observed precipitation towards the middle and end of the austral spring season. Figure 5d shows the climatological seasonal mean lower-level (850 hPa) circulation (streamlines) and 500 hPa vertical velocity (omega, shaded) for the pre-monsoon season (SON). The subtropical anti-cyclones over the Atlantic and Pacific Oceans, the low-level jet east of the Andes that is part of the prevailing anti-cyclonic circulation over South America and ascending vertical motion (indicated by negative omega values along the north-west–south-east precipitation band) are all highlighted, together with the two other upper-level features described above, as key components of the South American monsoon system. Figure 5 (first two rows) shows that both models satisfactorily represent most of these key elements, with CPC values above 0.97, omega pattern correlation (OPC) values above 0.60 and PPC values above 0.85 (except the Bolivian high, which is weakly formed in the two models – see Section 7 for discussion), despite some biases in precipitation and vertical velocity as illustrated in Figure 6 (first two rows). This latter figure shows good consistency between biases of these two variables, as regions presenting positive precipitation biases coincide with regions presenting negative omega (ascending vertical motion) biases, and regions presenting negative precipitation biases coincide with regions presenting positive omega (descending vertical motion) biases.

Figures 5g and 5j show similar circulation and precipitation plots to Figures 5a and 5d but now for the peak monsoon season (DJF). These figures shows that all above described elements of the South American monsoon system previously identified during the pre-monsoon season (SON) are also identified during the peak monsoon season (DJF), namely the north-west–south-east precipitation band over central South America and associated ascending vertical motion, the Bolivian High circulation and north-eastern South America trough at upper levels (200 hPa), the subtropical anti-cyclones over the Atlantic and Pacific Oceans at lower levels (850 hPa) and the low-level jet east of the Andes. Both models adequately represent all these

elements, with CPC values above 0.98, OPC values above 0.76 and PPC values above 0.87, despite precipitation and vertical velocity biases as illustrated in Figure 6 (last two rows).

Figure 7 shows the climatological (1981–2010) seasonal mean sea level pressure (shaded) and 850 hPa vector wind (arrows) for the pre-monsoon (SON, first row) and peak monsoon (DJF, second row) computed using observations (first column, ERA5) and the ensemble means of the two investigated climate models [second column (BAM-1.2) and third column (HadGEM3)]. The main features in this figure are the subtropical South Atlantic and Pacific high-pressure systems over the oceans surrounding the South America continent concentric with two 850 hPa anti-cyclones. Figure 7 shows that the two investigated models represent these features satisfactorily during both the pre-monsoon (SON) and peak monsoon (DJF) seasons, with the model simulations reproducing the observed patterns. Both models show CPC and sea level pressure pattern correlation (SPC) values above 0.97. Note, however, that over the South Atlantic Ocean the high-pressure system and associated anti-cyclonic circulation is overestimated by the two models in both seasons, as illustrated by the biases shown in Figure 8. This South Atlantic overestimation feature manifests near the south-east South America region in BAM-1.2, which consistently shows negative precipitation biases (Figures 6a and 6e) because a strengthened high-pressure system inhibits precipitation. Figure 8 also shows that HadGEM3 predominantly underestimates pressure over South America, leading to positive precipitation biases over some regions (e.g., south-east South America) as shown in Figures 6b and 6f.

The regional Walker circulation is another key feature of the South American monsoon system. Figure 9 (first row) shows the austral spring (SON) climatological (1981–2010) seasonal mean outgoing longwave radiation (shaded) overlaid with velocity potential (isolines) and divergent wind (arrows, which represent the non-rotational component of the total wind field) at 200 hPa computed using observations (first column, ERA5) and the ensemble means of the two investigated climate models [second column (BAM-1.2) and third column (HadGEM3)]. Figure 9 (second row) shows the corresponding climatological (1981–2010) seasonal mean precipitable water (shaded, which represents the amount of water available in the atmosphere) overlaid with velocity potential (isolines) and divergent wind component (arrows) at 850 hPa. Figure 9 (third row) shows the corresponding vertical climatological (1981–2010) seasonal meridional mean (over the core monsoon region, between 10°S and 30°S) negated vertical velocity (omega in Pa·s⁻¹ and displayed as arrows) and specific humidity (shaded) profiles from 1000 to 10 hPa. Vertical velocity (omega) is plotted as a negated quantity to make arrows
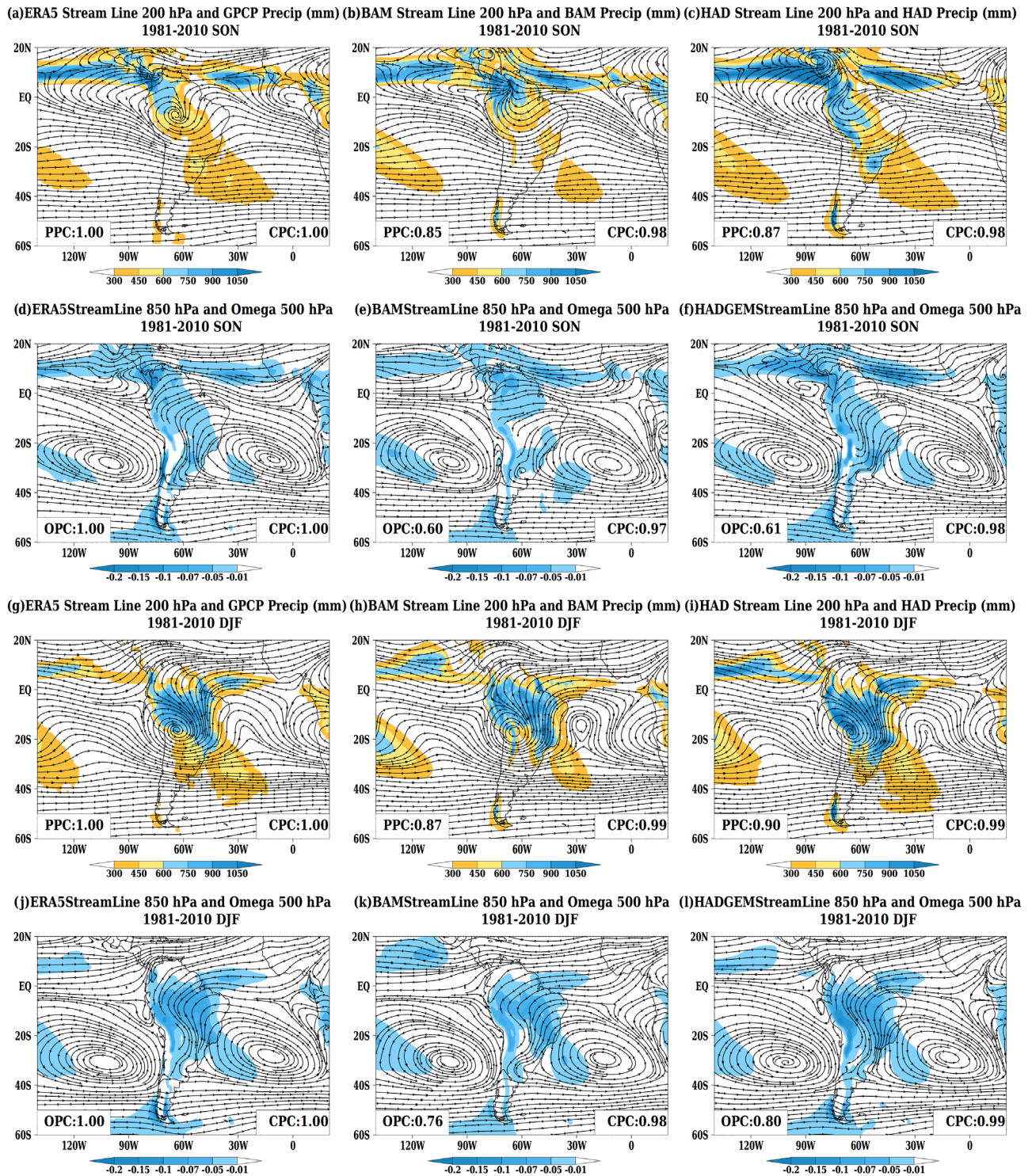
FIGURE 5   Climatological (1981–2010) seasonal mean 200 hPa circulation (streamlines) and accumulated seasonal precipitation (shaded, mm) for the austral spring (SON, first row) and summer (DJF, third row), and corresponding climatological seasonal mean 850 hPa circulation (streamlines) and 500 hPa vertical velocity (omega in Pa·s^{-1}, shaded) for the austral spring (SON, second row) and summer (DJF, fourth row), computed using observations (first column, GPCP v2.3 and ERA5) and the ensemble means of the two investigated climate models [second column (BAM-1.2) and third column (HadGEM3)]. The numbers at the bottom right corners of each panel are the circulation pattern correlation (CPC) values computed between the models and observed (ERA5) zonal and meridional wind components values used to produce these figure panels. The numbers at the bottom left corners of each panel are the precipitation pattern correlation (PPC) values or the vertical velocity (omega) pattern correlation (OPC) values computed between the models and observed (GPCP or ERA5) values shown in these figure panels
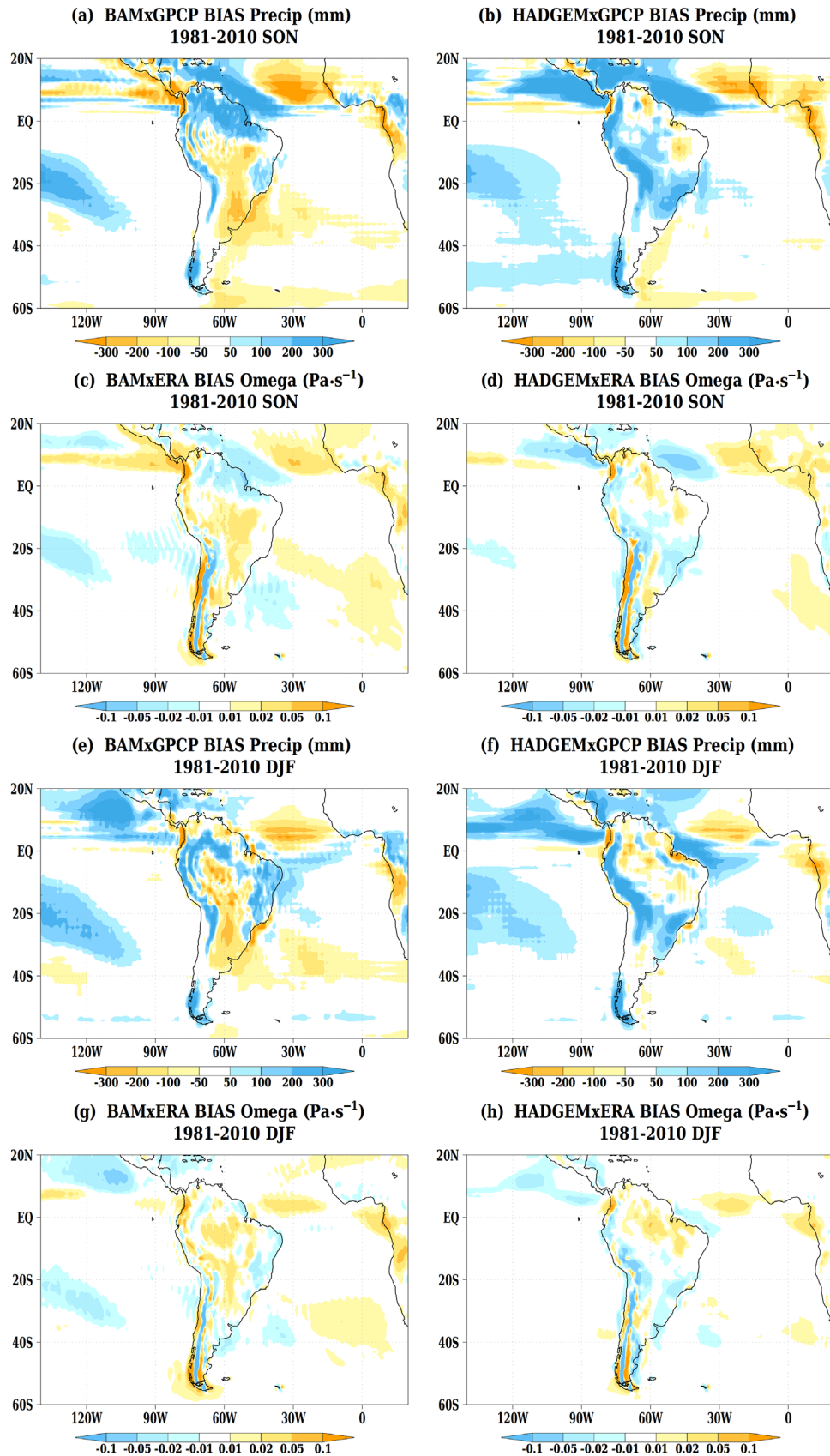
Climate Resilience and Sustainability
Interdisciplinary Approaches Towards Solutions for Climate Change   Open Access   RMetS

11

FIGURE 6 Precipitation (mm, first and third rows) and 500 hPa vertical velocity (omega, Pa·s^{-1}, second and fourth rows) biases for the austral spring (SON, first two rows) and summer (DJF, last two rows), computed for the ensemble means of the two investigated climate models [first column (BAM-1.2) and second column (HadGEM3)] with respect to GPCP v2.3 and ERA5 over the 1981–2010 period
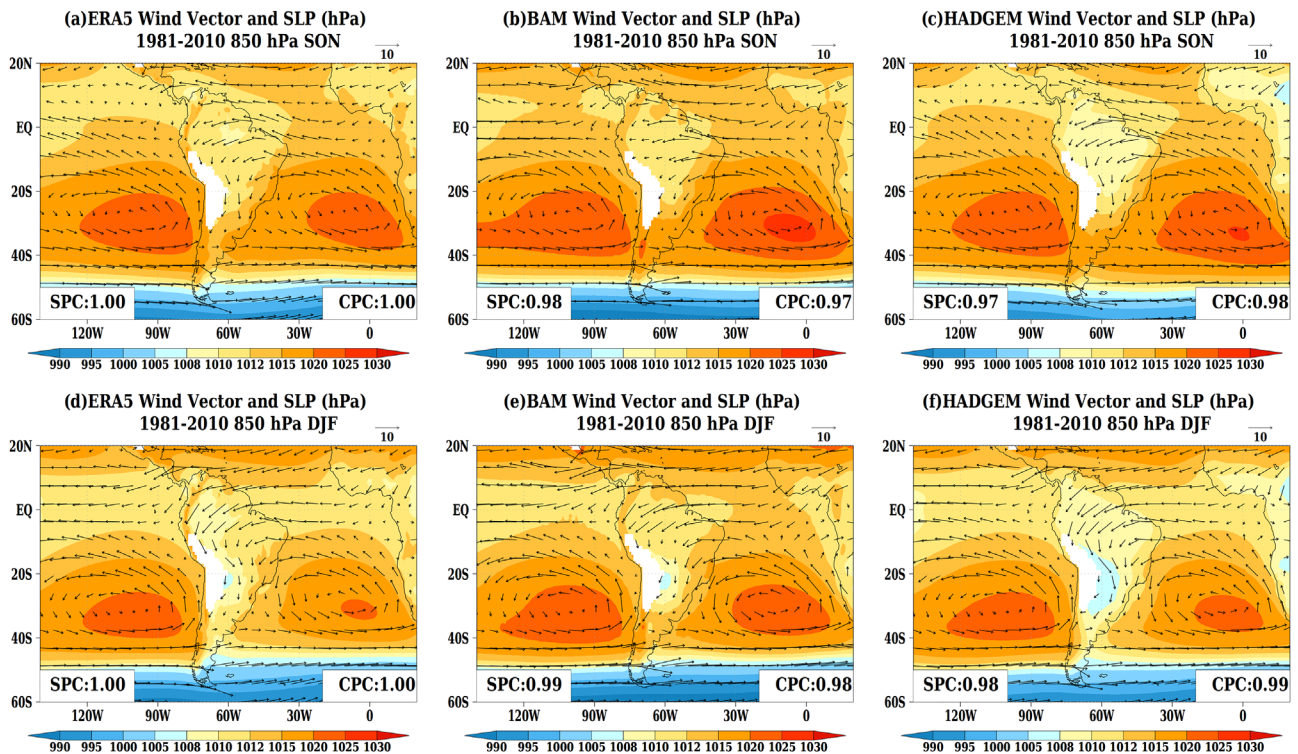
FIGURE 7 Climatological (1981–2010) seasonal mean sea level pressure (shaded, hPa) and 850 hPa vector wind (arrows, m·s^{-1}) for the austral spring (SON, first row) and summer (DJF, second row) computed using observations (first column, ERA5) and the ensemble means of the two investigated climate models [second column (BAM-1.2) and third column (HadGEM3)]. The numbers at the bottom right corners of each panel are the circulation pattern correlation (CPC) values computed between the models and ERA5 zonal and meridional wind components values used to produce these figure panels. The numbers at the bottom left corners of each panel are the sea level pressure pattern correlation (SPC) values computed between the models and ERA5 values shown in these figure panels

pointing upwards represent ascending vertical motion and arrows pointing downwards represent descending vertical motion.

Figure 9 (first and second rows) shows that the two models adequately represent the upper-level (200 hPa) divergence and lower-level (850 hPa) convergence over the core South American monsoon region, and the upper-level convergence and the lower-level divergence over the subtropical anti-cyclones in the Pacific and Atlantic. Both models show circulation (velocity potential) pattern correlation (CPC) values above 0.82. Figure 9 (first row) shows that despite the high outgoing longwave radiation pattern correlation (RPC) value of 0.95, pre-monsoon convection over South America (inferred from the outgoing longwave radiation) is weaker in BAM-1.2 than observed, which is consistent with the identified dry bias over this region (Figure 6a). Coelho et al. (2021) reported that this outgoing longwave radiation feature is due to BAM-1.2's atmosphere being more transparent than the real-world atmosphere, leading to misrepresentation of cloud–radiation interactions (see Section 7 for further discussion). Figure 9 (second and third rows) shows that humidity and precipitable water representation in both models resemble the obser-

vational reference, with precipitable water pattern correlation (PWPC) values above 0.98 and specific humidity pattern correlation (HPC) values above 0.99 in both models. However, Figure 9 (third row) illustrates that BAM-1.2 tends to underestimate humidity over the core monsoon region particularly at lower levels (around 925 hPa), and HadGEM3 also shows underestimation at higher levels (around 700 hPa). These features are also illustrated in panels a and b of Figure S3. Figure 9 (third row) shows that the Walker circulation with ascending motion over the core South American monsoon region and descending motion (subsidence) over the subtropical anti-cyclones in the Pacific and Atlantic is well simulated by both models, with vertical velocity (omega) pattern correlation (OPC) values above 0.86. However, panels a and b of Figure S3 show that the ascending motion over the core South American monsoon region is overestimated by BAM-1.2 around 850 hPa and by HadGEM3 around 700 hPa.

Figure 10 shows similar circulation, outgoing longwave radiation, precipitable water and humidity plots to Figure 9 but now for the peak monsoon season (DJF). The two models show circulation (velocity potential) pattern correlation (CPC) values above 0.90, outgoing longwave RPC values
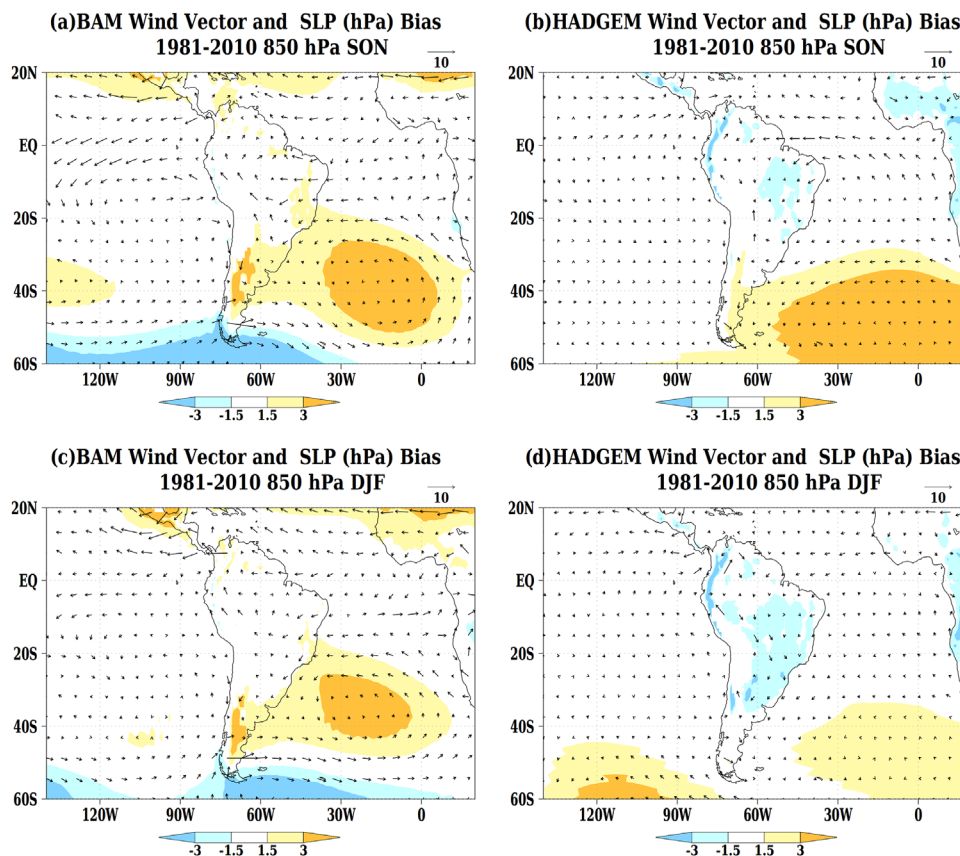
FIGURE 8 Sea level pressure (shaded, hPa) and 850 hPa vector wind (arrows, m·s^{-1}) biases for the austral spring (SON, first row) and summer (DJF, second row), computed for the ensemble means of the two investigated climate models [first column (BAM-1.2) and second column (HadGEM3)] with respect to ERA5 over the 1981–2010 period

above 0.93, PWPC values above 0.98 and specific HPC values above 0.99. The same upper and lower levels circulation features and model deficiencies previously identified for the pre-monsoon season (SON) in Figure 9 are also apparent in the peak monsoon season (DJF) when convection is enhanced over central South America. Both models adequately simulate the strengthened Walker circulation over the core regions of the South America monsoon system during DJF (Figure 10, third row) when compared to SON (Figure 9, third row), with vertical velocity (omega) pattern correlation (OPC) values above 0.95. Panels c and d of Figure S3 show similar specific humidity and vertical velocity biases for both models during the peak monsoon (DJF) to those identified in the pre-monsoon (SON) season (panels a and b of Figure S3).

5 | ASSOCIATIONS BETWEEN PRECIPITATION IN SOUTH-EAST BRAZIL AND ELSEWHERE IN SOUTH AMERICA

As previously illustrated in Figure 5 (first and third rows), a north-west–south-east-oriented precipitation band man-

ifests over central South America during both the pre-monsoon (SON) and peak monsoon (DJF) seasons. Over the continent, this band extended from the Amazon to south-east Brazil, in the region where the South Atlantic convergence zone is usually observed. This section investigates the associations between seasonal precipitation anomalies at the end of the continental portion of the above-mentioned band and its surroundings over South America during the 30-year period (1981–2010). Such a year-to-year seasonal precipitation variability analysis summarized by an association measure (the correlation coefficient) is important to further diagnose the spatial precipitation structure as represented in both observations and model simulations.

Figure 11 shows simultaneous correlations between the 1981–2010 time series of seasonal mean precipitation anomalies averaged over part of south-east Brazil (15°S–25°S, 40°W–50°W, illustrated by the squares in the maps) representing 30 values and the corresponding 1981–2010 time series of seasonal mean precipitation anomalies at each grid point over the study domain for the pre-monsoon (SON, first row) and peak monsoon (DJF, second row) seasons. The first column shows correlations computed using
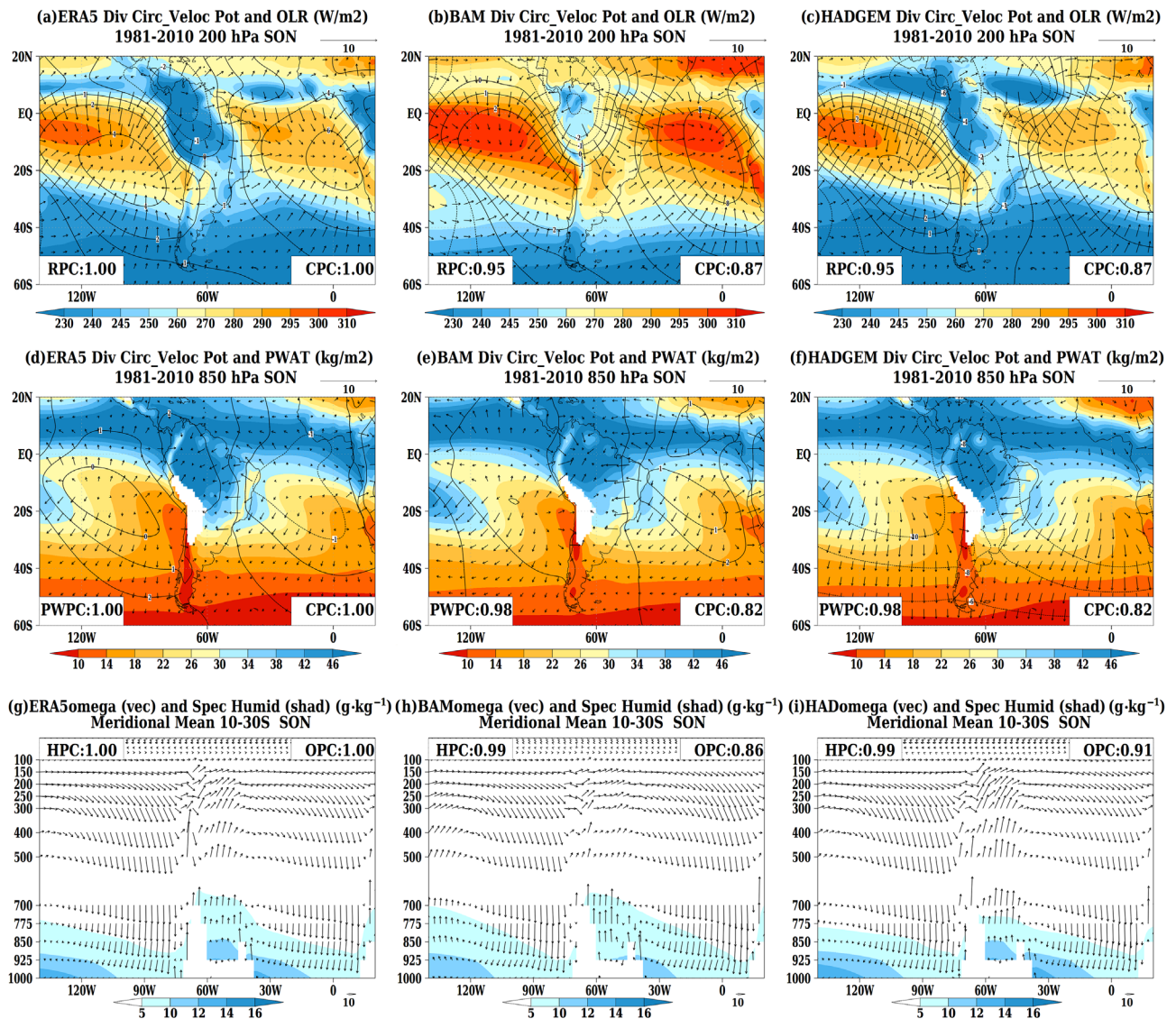
14 | Climate Resilience and Sustainability
Interdisciplinary Approaches Towards Solutions for Climate Change — Open Access — RMetS

COELHO ET AL.

FIGURE 9 Austral spring (SON) climatological (1981–2010) seasonal mean outgoing longwave radiation (OLR, shaded, W·m^{-2}) overlaid with velocity potential (isolines, 10^6 m^2·s^{-1}) and divergent wind (arrows, m·s^{-1}) at 200 hPa (first row) computed using observations (first column, ERA5) and the ensemble means of the two investigated climate models [second column (BAM-1.2) and third column (HadGEM3)]. Corresponding climatological (1981–2010) seasonal mean precipitable water (PWAT, shaded, Kg·m^{-2}) overlaid with velocity potential (isolines, 10^6 m^2·s^{-1}) and divergent wind (arrows, m·s^{-1}) at 850 hPa (second row). Corresponding vertical climatological (1981–2010) seasonal meridional mean (between 10°S and 30°S) negated vertical velocity (minus omega in Pa·s^{-1} × 10^3 displayed as arrows) and specific humidity (shaded, g·Kg^{-1}) profiles from 1000 to 10 hPa. The numbers at the bottom right corners of each panel in the first two rows are the circulation (velocity potential) pattern correlation (CPC) values computed between the models and ERA5 values. The numbers at the bottom left corners of each panel in the first two rows are the outgoing longwave radiation pattern correlation (RPC) values and precipitable water pattern correlation (PWPC) values computed between the models and ERA5 values. The numbers at the top right corners of each panel in the third row are the vertical velocity (omega) pattern correlation (OPC) values computed between the models and ERA5 values. The numbers at the top left corners of each panel in the third row are the specific humidity pattern correlation (HPC) values computed between the models and ERA5 values

observations (GPCP v2.3). The second and third columns show correlations computed using the ensemble means of the two investigated climate models (BAM-1.2 and HadGEM3, respectively). Figure 11a shows that during the pre-monsoon season (SON), precipitation anomalies over the investigated region in south-east Brazil are positively

associated with precipitation in neighbouring grid points, resulting in a north-west–south-east-oriented correlation pattern, which is aligned with the above-described precipitation band. These positive correlation values indicate consistency between the occurrence of positive (or negative) precipitation anomalies in the investigated region
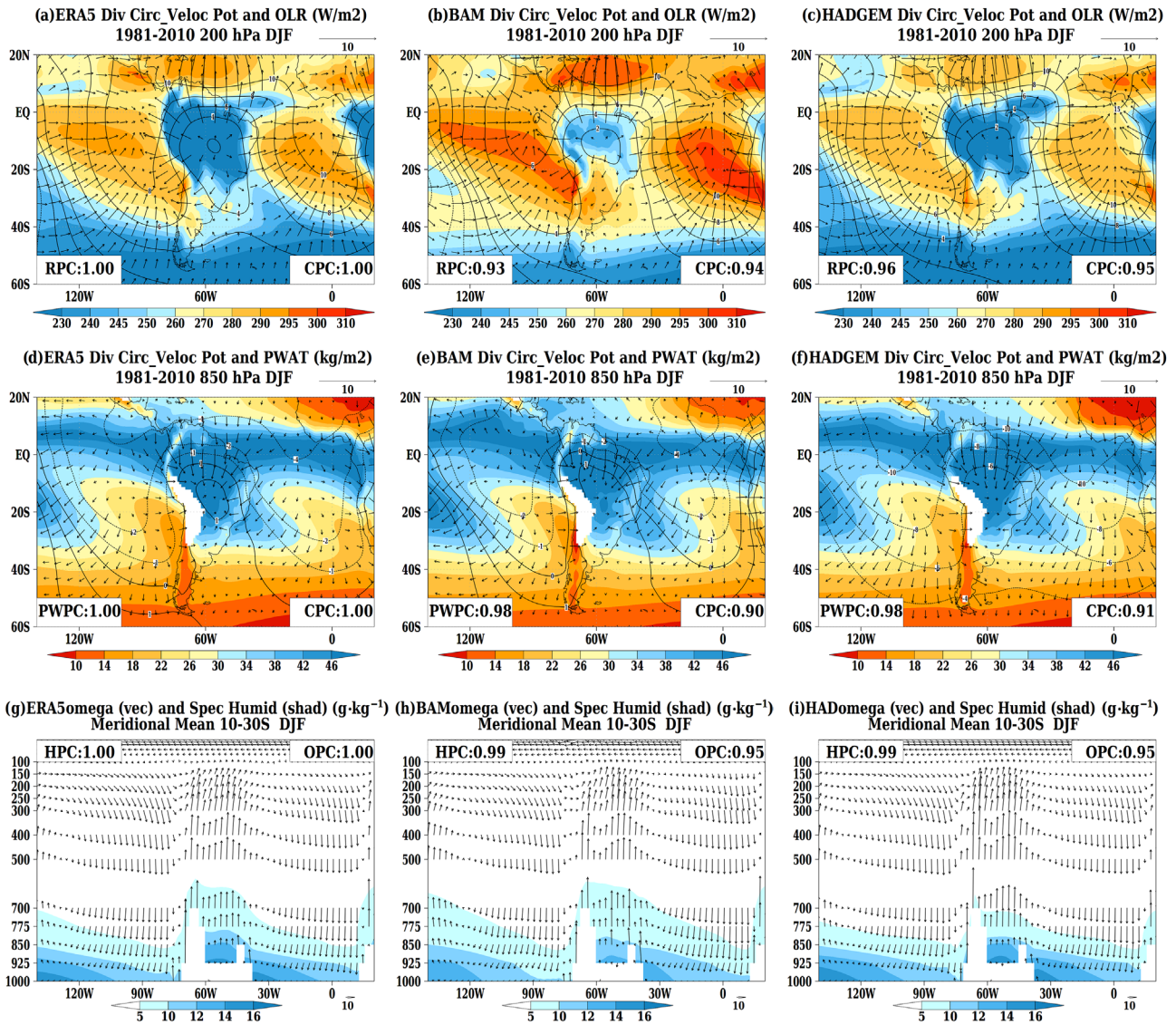
FIGURE 10 Same as Figure 9 but for austral summer (DJF)

and precipitation anomalies of the same sign in the surrounding grid points defining a north-west–south-east-oriented band of excess (or deficient) precipitation. Figures 11b and 11c show that the two investigated models reproduce this positive north-west–south-east-oriented correlation pattern, but also show negative correlation values in part of south Brazil, Uruguay and north-eastern Argentina. This negative correlation feature is not present in the observations (Figure 11a). Both models tend to overestimate the spatial extent of the above-described positive north-east–south-east-oriented correlation pattern, particularly over the ocean.

Figure 11d shows a similar feature occurring during the peak monsoon (DJF) season, with a north-west–south-east-oriented positive correlation pattern over the analysis region in south-east Brazil, but now also depicting neg-

ative correlation values over south-eastern South America (a region including part of the south region of Brazil, Uruguay and north-east Argentina). The opposite correlation values between these two regions indicate consistency between precipitation excess in one region occurring simultaneously with precipitation deficit in the other region. This austral summer spatial configuration has been documented in the literature as a dipole-like pattern (Nogues-Paegle and Mo, 1997; Vera et al., 2006; Gonzalez and Vera, 2014) representing excess precipitation over south-east Brazil and deficient precipitation over southeastern South America when the South Atlantic convergence zone is active and the opposite precipitation conditions over these two regions when the convergence zone is inactive. Ascending motion and convection are observed over the south-east Brazil region, where the South Atlantic
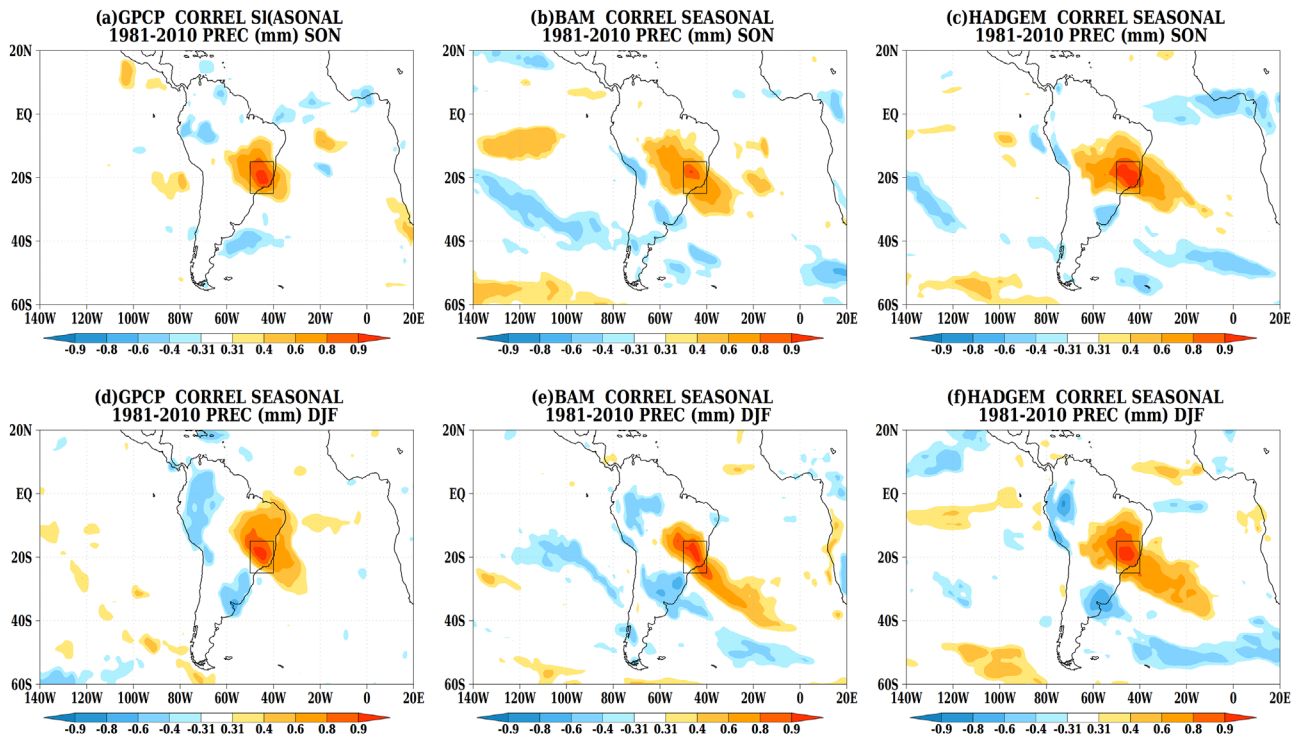
FIGURE 11 Simultaneous correlation between the 1981–2010 time series of seasonal mean precipitation anomalies averaged over part of south-east Brazil region (15°S–25°S, 40°W–50°W, illustrated by the squares drawn on the maps) and the 1981–2010 time series of seasonal mean precipitation anomalies at each grid point over the study domain for austral spring (SON, first row) and summer (DJF, second row). The first column shows correlation values computed using observations (GPCP v2.3). The second and third columns show correlation values computed using the ensemble means of the two investigated climate models (BAM-1.2 and HadGEM3, respectively). Correlation values above 0.31 or below –0.31 are statistically significant and different from zero using the Student's *t*-test at the 5% level

convergence zone manifests, and compensating descending motion (subsidence) prevails over south-eastern South America. Figures 11e and 11f show that both investigated models reproduce this dipole-like correlation pattern, and as identified for the pre-monsoon season (SON, Figures 11c and 11d) both models also tend to overestimate the spatial extent of these patterns particularly over the South Atlantic Ocean.

6 | CLIMATOLOGICAL DISTRIBUTIONS OF RAINY SEASON ONSET AND DEMISE DATES OVER SOUTH-EAST BRAZIL AND THE CORE SOUTH AMERICA MONSOON REGION

The characterization of rainy season onset and demise timing is another important aspect of the South American monsoon system that deserves investigation. This section assesses how well the two investigated models represent the climatological distributions of rainy season onset and demise dates over south-east Brazil (15°S–25°S, 40°W–50°W) and the core South America monsoon

region (10°S–20°S, 45°W–55°W) when compared to the observations.

The rainy season onset and demise dates for these two regions were determined following the method described in Liebmann et al. (2007), which is similar to the method proposed by Camberlin and Diop (2003). This method has been used for diagnostic and prognostic studies (e.g., Coelho et al., 2016; Coelho et al., 2017) and consists of searching for minimum and maximum values of smoothed anomalous daily precipitation accumulation curves, with accumulation starting on 1 July of each year (i.e. a few months prior to onset date). The date when the minimum value of this curve is identified represents an estimate for the onset date. The date when the maximum value of this curve is identified represents an estimate for the demise date. Applying this method for the observed and model simulated daily precipitation averaged over a particular region during the 1997/1998 to 2013/2014 period for which GPCP v1.3 daily data (Huffman et al., 2001) are available, one can construct climatological PDFs of onset and demise dates as illustrated in Figures 12 and 13.

Figure 12 shows kernel PDFs of rainy season onset (first row) and demise (second row) dates computed for the
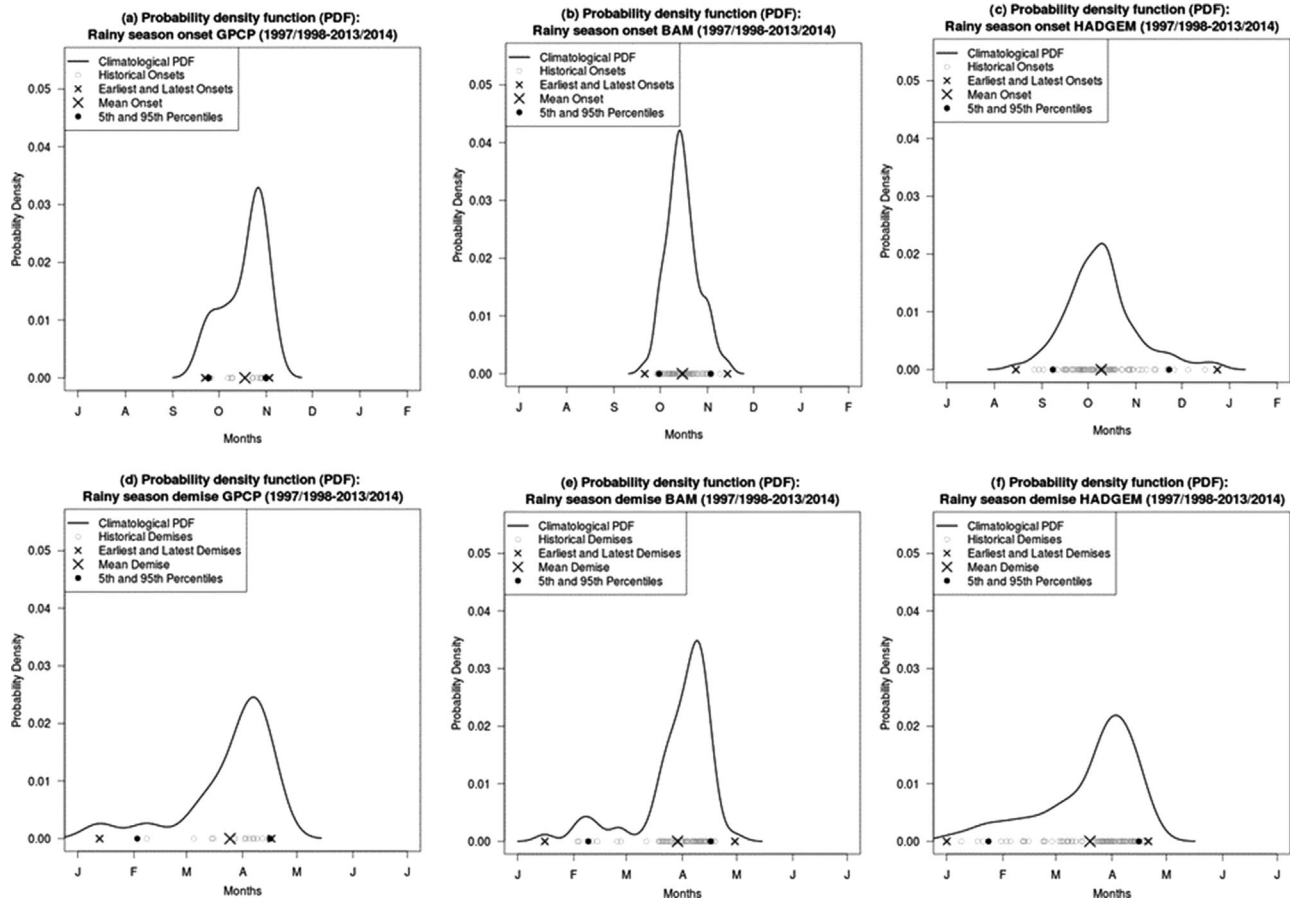
FIGURE 12 Probability density functions (PDFs) of rainy season onset (first row) and demise (second row) dates computed for the average precipitation over part of the south-east Brazil region (15°S–25°S, 40°W–50°W). The first column shows PDFs constructed using observations (GPCP v1.3). The second and third columns show PDFs using the individual ensemble members of the two investigated climate models (BAM-1.2 and HadGEM3, respectively). Grey circles are historical dates for the 17-year period from 1997/1998 to 2013/2014. The four BAM-1.2 ensemble members lead to a total of 68 dates (grey circles). The five HadGEM3 ensemble members lead to a total of 85 dates (grey circles). The solid lines are the kernel PDFs for the historical dates (grey circles). The large cross is the historical mean date computed over the 1997/1998 to 2013/2014 period. The small crosses are the earliest and latest onset and demise dates observed or simulated in the 1997/1998 to 2013/2014 period. The black dots are the 5th and 95th percentiles of observed or simulated onset and demise dates computed over the same period

average precipitation over part of the south-east Brazil region (15°S–25°S, 40°W–50°W) illustrated by the squares drawn on the South America maps shown on the top left corner of Figure 1b and in Figure 11. The first column shows PDFs constructed using observations (GPCP v1.3). The second and third columns show PDFs using the individual ensemble members of the two investigated climate models (BAM-1.2 and HadGEM3, respectively). Grey circles are historical dates for the 17-year period from 1997/1998 to 2013/2014, which are the actual individual dates for each year. The four BAM-1.2 ensemble members lead to a total of 68 dates (grey circles). The five HadGEM3 ensemble members lead to a total of 85 dates (grey circles). The solid lines are the kernel PDFs for the historical dates (grey circles). The spread of these grey circles and the width

of the kernel PDFs provide an indication about the interannual variability of onset and demise dates. The large cross is the historical mean date computed over the 1997/1998 to 2013/2014 period. The small crosses represent the earliest and latest onset and demise dates observed or simulated in the 1997/1998 to 2013/2014 period. The black dots represent the 5th and 95th percentiles of observed or simulated onset and demise dates computed over the same period.

Figure 12 (first row) shows that the historical mean onset over the south-east Brazil region (15°S–25°S, 40°W–50°W) is estimated to occur around 18 October (large cross in Figure 12a and Table 2). BAM-1.2 simulates the historical mean onset date (large cross in Figure 12b and Table 2) around 15 October, whereas HadGEM3 tends to simulate the historical mean onset date slightly earlier than
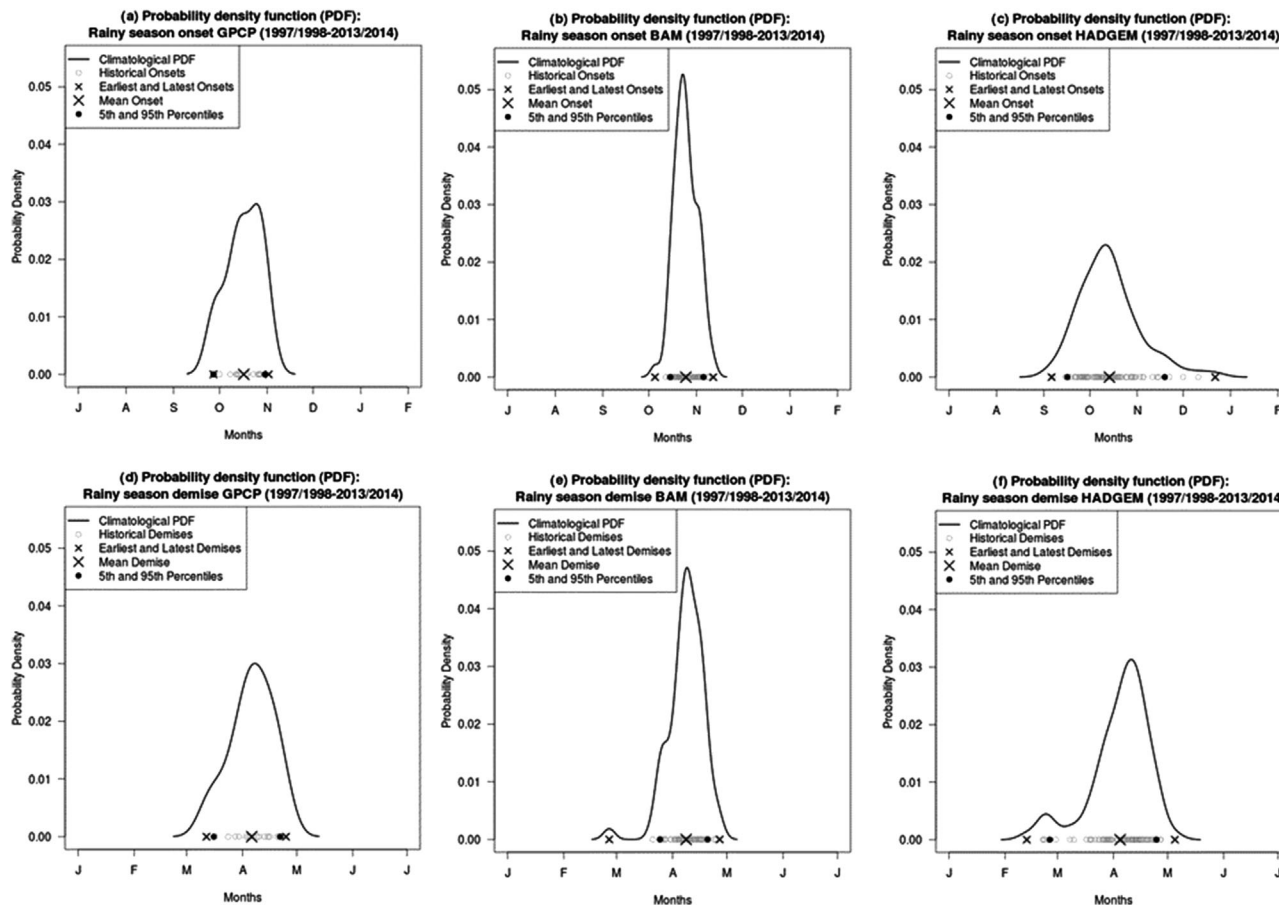
FIGURE 13 Probability density functions (PDFs) of rainy season onset (first row) and demise (second row) dates computed for the average precipitation over the core South American monsoon region (10°S–20°S, 45°W–55°W). The first column shows PDFs constructed using observations (GPCP v1.3). The second and third columns show PDFs using the individual ensemble members of the two investigated climate models (BAM-1.2 and HadGEM3, respectively). Grey circles are historical dates for the 17-year period from 1997/1998 to 2013/2014. The four BAM-1.2 ensemble members lead to a total of 68 dates (grey circles). The five HadGEM3 ensemble members lead to a total of 85 dates (grey circles). The solid lines are the kernel PDFs for the historical dates (grey circles). The large cross is the historical mean date computed over the 1997/1998 to 2013/2014 period. The small crosses are the earliest and latest onset and demise dates observed or simulated in the 1997/1998 to 2013/2014 period. The black dots are the 5th and 95th percentiles of observed or simulated onset and demise dates computed over the same period

TABLE 2 Statistic for the climatological (1997/1998 to 2013/2014) onset and demise dates including the earliest, the 5th percentile, the mean, the 95th percentile and the latest dates, for average precipitation over part of the south-east Brazil region (15°S–25°S, 40°W–50°W), for the observations (GPCP v1.3) and the two investigated model ensemble simulations (BAM-1.2 and HadGEM3)

South-east region (15°S–25°S, 40°W–50°W)	Earliest	5th percentile	Mean	95th percentile	Latest
Onset dates					
GPCP	22 September	24 September	18 October	31 October	3 November
BAM	21 September	30 September	15 October	3 November	14 November
HADGEM	15 August	8 September	9 October	22 November	24 December
Demise dates					
GPCP	13 January	2 February	25 March	16 April	17 April
BAM	16 January	9 February	29 March	16 April	30 April
HADGEM	1 January	24 January	19 March	15 April	21 April

TABLE 3 Statistic for the climatological (1997/1998 to 2013/2014) onset and demise dates including the earliest, the 5th percentile, the mean, the 95th percentile and the latest dates, for average precipitation over the core South American monsoon region (10°S–20°S, 45°W–55°W), for the observations (GPCP v1.3) and the two investigated model ensemble simulations (BAM-1.2 and HadGEM3)

Core region (10°S–20°S, 45°W–55°W)	Earliest	5th percentile	Mean	95th percentile	Latest
Onset dates					
GPCP	27 September	27 September	16 October	30 October	2 November
BAM	5 October	15 October	25 October	5 November	12 November
HADGEM	6 September	16 September	13 October	19 November	22 December
Demise dates					
GPCP	12 March	16 March	6 April	21 April	25 April
BAM	26 February	25 March	8 April	20 April	27 April
HADGEM	13 February	25 February	4 April	24 April	5 May

observed, around 9 October (large cross in Figure 12b and Table 2). These figures and Table 2 also illustrate that BAM-1.2 has a closer representation of the interannual variability in onset dates to the observations than HadGEM3, including the estimation of the earliest and latest onset dates (small crosses) and of the 5th and 95th percentiles (black dots), with a narrower kernel PDF for BAM-1.2 that resembles the observed kernel PDF. However, the BAM-1.2 kernel PDF (Figure 12b) shows a secondary peak after the main peak, whereas the observed kernel PDF (Figure 12a) shows a secondary peak before the main peak, suggesting some differences between the simulated and observed interannual variability of onset dates. Figure 12 (second row) and Table 2 show that the historical mean demise over the south-east Brazil region (15°S–25°S, 40°W–50°W) is estimated to occur around 25 March (large cross in Figure 12d). BAM-1.2 simulates the historical mean demise date (large cross in Figure 12e) slightly later than the estimated date around 29 March, whereas HadGEM3 tends to simulate the historical mean demise date slightly earlier than observed around 19 March (large cross in Figure 12f). These figures also illustrate that both models show similar interannual variability in demise dates to the observations, as their kernel PDFs resemble the observed kernel PDF.

Figure 13 shows a similar onset and demise kernel PDFs to Figure 12 but now for dates computed with average precipitation over the core South American monsoon region (10°S–20°S, 45°W–55°W). Figure 13 (first row) shows that the historical mean onset is estimated to occur around 16 October (large cross in Figure 13a and Table 3). BAM-1.2 simulates the historical mean onset date (large cross in Figure 13b and Table 3) a few days later around 25 October, whereas HadGEM3 tends to simulate the historical mean onset date slightly earlier than observed around 13 October (large cross in Figure 13b and Table 3). These figures and Table 3 also illustrate that BAM-1.2 has all statistics indicating later dates when compared to the observa-

tions, including the estimation of the earliest and latest onset dates (small crosses) and of the 5th and 95th percentiles (black dots). HadGEM3 also has statistics indicating later dates when compared to the observations for the 95th percentile and latest onset dates, whereas for the 5th percentile and earliest onset dates HadGEM3 has statistics indicating earlier dates when compared to the observations. BAM-1.2 shows a narrower kernel PDF than HadGEM3, which despite having later than observed dates better resembles the observed kernel PDF. Figure 13 (second row) and Table 3 show that the historical mean demise over the core South American monsoon region (10°S–20°S, 45°W–55°W) is estimated to occur around 6 April (large cross in Figure 13d). BAM-1.2 simulates the historical mean demise date (large cross in Figure 12e) slightly later than the estimated date around 8 April, whereas HadGEM3 tends to simulate the historical mean demise date slightly earlier than observed around 4 April (large cross in Figure 13f). BAM-1.2 shows a kernel PDF slightly narrower than the observed kernel PDF, whereas HadGEM3 shows a kernel PDF slightly wider than the observed kernel PDF, illustrating model deficiencies in simulating demise dates interannual variability.

However, it is recognized that there are differences in onset and demise dates characteristics between the east and west borders of these two regions here investigated. Future work mapping spatially varying statistics of onset and demise dates PDFs shown here would be an important extension of the study.

7 | DISCUSSIONS AND CONCLUSIONS

This study aimed at assessing the ability of a Brazilian (BAM-1.2; Coelho et al., 2021) and a UK (HadGEM3; Ridley et al., 2018; Williams et al., 2018) climate model to represent the main features of the South American

20 | Climate Resilience and Sustainability
Interdisciplinary Approaches Towards Solutions for Climate Change Open Access | RMetS

COELHO ET AL.

Monsoon system. Climatological ensemble means of AMIP-type climate simulations computed over the period 1981–2010 were evaluated. The assessment evaluated the ability of the models to represent the South America austral summer and winter precipitation contrast and associated circulation, key elements of the South American monsoon system during austral spring and summer, the association between south-east Brazil and South America precipitation and climatological distributions of rainy season onset and demise dates over south-east Brazil (15°S–25°S, 40°W–50°W) and the core monsoon region (10°S–20°S, 45°W–55°W), the latter assessed over the 1997/1998 to 2013/2014 period. Our results show that the two investigated models were able to represent to a large extent the main features of the South America Monsoon system, though some notable discrepancies between models and observations were identified. This section summarizes the key strengths of each model and explores possible physical reasons for why model behaviour sometimes deviates from observations.

Both models depicted the monsoon region and adequately represented the main monsoon features, including (1) the north-west–south-east precipitation band and associated ascending vertical motion over central South America; (2) the upper-level Bolivian High circulation and the north-east South America trough during the summer; (3) the lower-level South Atlantic and Pacific subtropical anti-cyclones and (4) the low-level jet east of the Andes. Both models consistently represented upper-level divergence and lower-level convergence over the core monsoon region, and the upper-level convergence and the lower-level divergence over the anti-cyclones in the Pacific and Atlantic associated with the regional Walker circulation during both the pre-monsoon (spring) and peak monsoon (summer) seasons. The two models reproduced the dipole-like precipitation pattern between south-east Brazil and south-eastern South America (Nogues-Paegle and Mo, 1997; Vera et al., 2006; Gonzalez and Vera, 2014) during the austral summer but overestimate the spatial extent of these patterns particularly over the South Atlantic. Both models simulated the main observed climatological features of both rainy season onset and demise dates for the two investigated regions (south-east Brazil and the core South American monsoon region), although HadGEM3 overestimates the interannual variability of onset dates.

The upper-level anticyclonic circulation, the Bolivian high, is well developed during austral summer (DJF), as discussed by Silva Dias et al. (1983), Figueroa et al. (1995), Lenters and Cook (1997), and others. Its formation is due to long Rossby wave westward propagation associated with latent heat released by deep convective activity (Silva Dias et al., 1983), mainly over the Amazon basin and central Brazil (Lenters and Cook, 1997). This upper-level circula-

tion is not observed during the austral winter (JJA) due to the lack of deep convective activity. On the other hand, during the austral spring (SON), a weaker upper-level anticyclonic circulation is observed, as shown in Figure 5a. The weaker Bolivian high during spring (SON) when compared to the strength of the Bolivian high during the summer (DJF) is due to the predominantly equatorial convective activity; therefore, a weak Rossby wave westward propagation compared to the Kevin wave response. The weak Bolivian high simulation as identified in both investigated models during SON is likely to be related to the errors in representing convective precipitation around the equatorial region, mainly over north-western South America, where the Andes Mountains directly impact the models' circulation simulations in terms of mass convergence, divergence and vertical waves propagation through all atmospheric column levels. Therefore, models' deficiencies in representing these circulation features would be affecting the model's ability to simulate convective precipitation during SON. In contrast, the models adequately simulated the Bolivian high during DJF because convective precipitation over the Amazon Basin and central Brazil is well represented.

The excessive outgoing longwave radiation feature identified in BAM-1.2 under cloudy conditions has been reported to be related to insufficient absorption of longwave radiation from lower and warmer atmospheric layers (Coelho et al., 2021). In other words, the model's atmosphere is more transparent than the observations (i.e. clouds have a lower optical depth than observed), leading to misrepresentation of cloud–radiation interactions. As reported in Cavalcanti et al. (2020) and Coelho et al. (2021), underestimation of convective clouds also contributes to the overestimation of outgoing longwave radiation over the Amazon region. Even though the model's atmosphere contains close to the observed amount of moisture, as illustrated by the precipitable water maps in Figures 9 and 10, simulated clouds might be misplaced in altitude. This latter feature is also a possible contributing factor to the excessive simulated outgoing longwave radiation over South America. Besides, under clear-sky conditions the model longwave radiation closely agrees with the observations (Coelho et al., 2021), reinforcing the hypothesis of misrepresentation of cloud optical properties and cloud–radiation interactions in the model. All these deficiencies point to the need to investigate new approaches for representing clouds in the model in order to improve cloud optical properties and parameters such as cloud fraction and liquid and ice water content.

Documenting the ability of climate models to capture observed climate conditions is important to support their use for studying the impacts of climate and land-use change. In particular, there is urgent need for accurate

COELHO ET AL.

Climate Resilience and Sustainability
Interdisciplinary Approaches Towards Solutions for Climate Change   Open Access   RMetS   21

future precipitation projections in order to improve societal resilience to climate change, recommend strategies for climate adaptation and identify solutions. Such recommendations and policies include the preservation of forests (a) to maintain functional biosphere–atmosphere interactions, essential for the South America monsoon system's hydrological cycle, and (b) to increase the diversification of power generation systems to include additional renewable energy sources (e.g. solar and wind power production plants). The latter will contribute to make the predominant South America hydropower production system less vulnerable to year-to-year climate variability, because prolonged periods of precipitation deficit, as experienced in a large portion of the continent at the time of written, directly affect the region's energy production capability.

Results from this study show BAM-1.2 and HadGEM3 are capable of simulating the key elements of the South American monsoon system, providing confidence in their use in future research to help society deal with South American monsoon climate variability and its associated impacts. Where model deficiencies were identified, these can be used to drive model development and further improve predictive capabilities.

ORCID

Caio A. S. Coelho https://orcid.org/0000-0002-9695-5113
Amulya Chevuturi https://orcid.org/0000-0003-2815-7221

REFERENCES

Adler, R.F., Huffman, G.J., Chang, A., Ferraro, R., Xie, P., Janowiak, J. et al. (2003) The version 2 Global Precipitation Climatology Project (GPCP) monthly precipitation analysis (1979-present). *Journal of Hydrometeorology*, 4, 1147–1167.

Baker, J.C.A., de Souza, D.C., Kubota, P., Buermann, W., Coelho, C.A.S., Andrews, M.B. et al. (2021) An assessment of land-atmosphere interactions over South America using satellites, reanalysis and two global climate models. *Journal of Hydrometeorology*, 22(5), 1333–1350.

Barichivich, J., Gloor, E., Peylin, P., Brienen, R.J.W., Schöngart, J., Espinoza, J.C., et al. (2018): Recent intensification of Amazon flooding extremes driven by strengthened Walker circulation. *Science Advances*, 4, eaat8785.

Camberlin, P. & Diop, M., (2003): Application of daily rainfall principal component analysis to the assessment of the rainy season characteristics in Senegal. *Clim. Res.*, 23, 159–169

Carvalho, L.M.V. & Cavalcanti, I.F.A. (2016) The South American monsoon system. In: de Carvalho, L.M.V. & Jones, C. (Eds.) *The monsoons and climate change: observations and modeling*. Cham, Switzerland: Springer, pp. 121–148.

Cavalcanti, I.F.A. & Raia, A., (2017): Lifecycle of South American monsoon system simulated by CPTEC/INPE AGCM. *International Journal of Climatology*, 37, 878–896.

Cavalcanti, I.F.A., Silveira, V.P., Figueroa, S.N., Kubota, P.Y., Bonatti, J.P. & de Souza, D.C., (2020) Climate variability over South America – regional and large scale features simulated by the Brazilian Atmospheric Model (BAM-v0). *International Journal of Climatology*, 40, 2845–2869.

Coelho, C.A.S., Cardoso, D.H.F & Firpo, M.A.F., (2016): Precipitation diagnostics of an exceptionally dry event in São Paulo, Brazil. *Theoretical and Applied Climatology*, 125(3), 769–784.

Coelho, C.A.S., Firpo, M.A.F., Maia, A.H.N. & MacLachlan, C., (2017): Exploring the feasibility of empirical, dynamical and combined probabilistic rainy season onset forecasts for São Paulo,

22 Climate Resilience and Sustainability
Interdisciplinary Approaches Towards Solutions for Climate Change · Open Access · RMetS

COELHO ET AL.

Brazil. *International Journal of Climatology*, 37(S1), 398–411. https://doi.org/10.1002/joc.5010

Coelho, C.A.S., de Souza, D.C., Kubota, P.Y., Costa, S.M.S., Menezes, L., Guimaraes, B.S., et al. (2021): Evaluation of climate simulations produced with the Brazilian global atmospheric model version 1.2. *Climate Dynamics*, 56, 873–898. https://doi.org/10.1007/s00382-020-05508-8

Díaz, L.B., Saurral, R.I. & Vera, C.S., (2020): Assessment of South America summer rainfall climatology and trends in a set of global climate models large ensembles. *Int. Journ. Climat.*, 41, E59-E77. https://doi.org/10.1002/joc.6643

Espinoza, J.C., Ronchail, J., Guyot, J.L., Junquas, C., Vauchel, P., Lavado, W., et al. (2011): Climate variability and extreme drought in the upper Solimões River (western Amazon Basin): understanding the exceptional 2010 drought. *Geophysical Research Letters*, 38, 1–6.

Figueroa, S.N., Satyamurty, P. & Da Silva Dias, P.L., (1995): Simulations of the summer circulation over the South American region with an eta coordinate model. *Journal of Atmospheric Science*, 52, 1573–1584.

Gan, M.A., Kousky, V.E. & Ropelewski, C.F., (2004) The South America monsoon circulation and its relationship to rainfall over West-Central Brazil. *J Clim*, 17, 47–66.

García-Franco, J.L., Gray, L.J. & Osprey, S., (2020) The American monsoon system in HadGEM3 and UKESM1. *Weather Clim. Dyn.*, 1, 349–371. https://doi.org/10.5194/wcd-1-349-2020.

Gonzalez, P.L.M & Vera, C.S., (2014): Summer precipitation variability over South America on long and short intraseasonal timescales. *Climate Dynamics*, 43, 1993–2007

Hersbach, H., Bell, B., Berrisford, P., Hirahara, S., Horányi, A., Muñoz-Sabater, J., et al. (2020): The ERA5 global reanalysis. *Quarterly Journal of the Royal Meteorological Society*, 146, 1999–2049.

Huffman, G.J., Adler, R.F., Morrissey, M., Bolvin, D.T., Curtis, S., Joyce, R., et al. (2001): Global Precipitation at One-Degree Daily Resolution from Multi-Satellite Observations. *J. Hydrometeor.*, 2(1), 36–50.

Jones, C. & Carvalho, L.M.V., (2002): Active and break phases in the South American Monsoon System. *J. Clim.*, 15, 905–914.

Jones, C. & Carvalho, L.M.V., (2013): Climate change in the South American monsoon system: present climate and CMIP5 projections. *J Clim*, 26, 6660–6678

Kitoh, A., Endo, H., Kumar, K.K., Cavalcanti, I.F.A., Goswami, P. & Zhou, T.J., (2013): Monsoons in a changing world: a regional perspective in a global context. *Journal of Geophysical Research: Atmospheres*, 118, 3053–3065.

Kodama, Y., (1992): Large-scale common features of subtropical precipitation zones (the Baiu Frontal Zone, the SPCZ, and the SACZ) Part I: characteristics of subtropical frontal zones. *J Meteorol Soc Japan*, 70, 813–836. https://doi.org/10.1248/cpb.37.3229

Kodama, Y-M., (1993): Large-scale common features of sub-tropical convergence zones (the Baiu Frontal Zone, the SPCZ, and the SACZ) Part II: conditions of the circulations for generating the STCZs. *J Meteorol Soc Japan*, 71, 581–610. https://doi.org/10.1248/cpb.37.3229

Kousky, V.E., (1988): Pentad outgoing longwave radiation climatology for the South American sector. *Rev Bras Met*, 3, 217–231.

Lenters, J.D. & Cook, K.H. (1997): On the origin of the Bolivian high and related circulation features of the South American climate. *Journal of the Atmospheric Sciences*, 54, 656–678.

Liebmann, B. & Marengo, J., (2001): Interannual variability of the rainy season and rainfall in the Brazilian Amazon basin. *J Clim*, 14, 4308–4318.

Liebmann, B., Camargo, S.J., Seth, A., Marengo, J.A., Carvalho, L.M.V., Allured, D., et al. (2007): Onset and end of the rainy season in South America in observations and the ECHAM 4.5 atmospheric general circulation model. *J. Clim.*, 20, 2037–2050.

Marengo, J.A., Soares, W.R., Saulo, C. & Nicolini, M., (2004): Climatology of the low-level jet east of the Andes as derived from the NCEP-NCAR reanalyses: characteristics and temporal variability. *Journal of Climate*, 17(12), 2261-2280

Marengo, J.A., Nobre, C.A., Tomasella, J., Oyama, M.D., Sampaio De Oliveira, G., De Oliveira, R., et al. (2008) The drought of Amazonia in 2005. *Journal of Climate*, 21, 495–516.

Marengo, J.A., Tomasella, J., Alves, L.M., Soares, W.R. & Rodriguez, D.A., (2011) The drought of 2010 in the context of historical droughts in the Amazon region. *Geophysical Research Letters*, 38, 1–5.

Marengo, J.A, Liebmann, B., Grimm, A.M., Misra, V., Silva Dias, P.L., Cavalcanti, I.F.A., et al. (2012): Recent developments on the South American monsoon system. *International Journal of Climatology*, 32, 1–21.

Marengo, J.A. & Espinoza, J.C., (2016) Extreme seasonal droughts and floods in Amazonia: causes, trends and impacts. *International Journal of Climatology*, 36, 1033–1050.

Nogues-Paegle, J. & Mo, K.C., (1997): Alternating wet and dry conditions over South America during summer. *Monthly Weather Review*, 125, 279–291.

Raia, A. & Cavalcanti, I.F.A., (2008): The life cycle of the South American monsoon system. *J. Clim.*, 21, 6227–6246.

Ridley, J., Menary, M., Kuhlbrodt, T., Andrews, M. & Andrews, T. (2018) *MOHC HadGEM3-GC31-LL model output prepared for CMIP6 CMIP*. Earth System Grid Federation. https://doi.org/10.22033/ESGF/CMIP6.6109

Silva, A.E. & Carvalho, L.M.V., (2007): Large-scale index for South America MONSOON (LISAM). *Atmospheric Science Letters*, 8, 51–57.

Silva Dias, P.L.; Schubert, W.H.; & De Maria, M. (1983): Large-scale response of the tropical atmosphere to transient convection. *J. Clim.*, 40, 2689–2707.

Silva, V.B.S. & Kousky, V.E. (2012) The South American monsoon system: climatology and variability. In: Wang, S.-Y. & Gillies, R. (Eds.) *Modern climatology*. Rijeka, Croatia: IntechOpen, pp. 123–152.

Vera, C., Higgins, W., Amador, J., Ambrizzi, T., Garreaud, R., Gochis, D., et al. (2006) Toward a unified view of the American monsoon systems. *Journal of Climate*, 19(20), 4977–5000. https://doi.org/10.1175/JCLI3896.1.

Wang, B., Kim, H-J., Kikuchi, K. & Kitoh, A., (2011): Diagnostic metrics for evaluation of annual and diurnal cycles. *Climate Dynamics*, 37, 941–955. https://doi.org/10.1007/s00382-010-0877-0

Williams, K.D., Copsey, D., Blockley, E.W., Bodas-Salcedo, A., Calvert, D., Comer, R., et al. (2018): The Met Office Global Coupled Model 3.0 and 3.1 (GC3.0 and GC3.1) Configurations. *Journal of Advances in Modeling Earth Systems*, 10, 357–380.

Zemp, D.C., Schleussner, C.F., Barbosa, H.M.J., van der Ent, R.J., Donges, J.F., Heinke, J., et al. (2014): On the importance of cascading moisture recycling in South America. *Atmospheric Chemistry and Physics*, 14, 13337–13359. https://doi.org/10.5194/acp-14-13337-2014

COELHO ET AL.

Climate Resilience and Sustainability
Interdisciplinary Approaches Towards Solutions for Climate Change | Open Access | RMetS | 23

Zeng, N., Yoon, J.-H., Marengo, J.A., Subramaniam, A., Nobre, C.A., Mariotti, A., et al. (2008): Causes and impacts of the 2005 Amazon drought. *Environmental Research Letters*, 3, 1–9.

Zhou, J. & Lau, K.M., (1998): Does a monsoon climate exist over South America? *J. Climate*, 11, 1020–1040.

SUPPORTING INFORMATION

Additional supporting information may be found in the online version of the article at the publisher's website.